

Hydrated Ionic Liquids with and without Solute: The Influence of Water Content and Protein Solutes

Michael Haberler, Christian Schröder, and Othmar Steinhauser*

University of Vienna, Department of Computational Biological Chemistry, Austria

S Supporting Information

ABSTRACT: In this computational study, the network of 1-ethyl-3-methylimidazolium trifluoromethanesulfonate/water mixtures is analyzed in the presence (and absence) of the protein ubiquitin and a zinc finger motif. Thereby, common radial distribution functions are decomposed into contributions from different Voronoi shells, and the mutual orientation of cations, anions, and water in the bulk phase as a function of the water mole fraction is discussed. Single particle translation and the reorientation of the dipolar axis seem to follow hydrodynamic relations. Using the body-fixed frame as an alternative reference system, translation and rotation can be decomposed into contributions along and about the axes of a well-defined orthogonal trihedron, thus elucidating the principal motions of the cations and anions as a function of the water mole fraction. The structural dipolar orientation may be correlated with single particle dynamics and can be characterized by the static collective Kirkwood order parameter.

I. INTRODUCTION

Molecular ionic liquids (IL) recently came to the fore as an interesting alternative to common organic solvents in a wide range of processes with biotechnological and industrial relevance, e.g., the dissolution of biomass in ionic liquids^{1,2} or the extraction of pharmaceutically active compounds by ionic liquids.³ They may even serve as pharmaceuticals themselves.⁴ In these applications, the interactions of the ionic liquid and the solute with water play a key role. In principle, water in the vicinity of biomolecules can be classified into three categories: (a) internal water buried in the biomolecular structure, (b) hydration water at the surface of the biomolecule, and (c) bulk or free water which, in principle, no longer perceives the influence of the dissolved biomolecule. This may exclude up to five hydration shells, even in pure aqueous protein solutions.^{5,6}

From the point of view of an aqueous protein solution, it is tempting to characterize ionic liquids as kosmotropic (strongly hydrogen bonded to water) or chaotropic (weakly hydrogen bonded) molecules,^{7–10} although their impact on the water structure seems stronger than nonionic kosmotropes or chaotropes.⁸ Kosmotropes are supposed to stabilize proteins because they mediate a strong hydrogen bond network including the water molecules, resulting in a decreased solubility of the hydrophobic parts of the protein, whereas chaotropes often unfold protein structure.⁹ In this sense, the effect of ionic liquids was analyzed in terms of “salting-in”, i.e., higher solubility of the protein with increasing ionic strength, or “salting-out”. Their relative strength was ranked in a “Hofmeister” series.^{11–13} However, recent studies cast doubt on a “simple” kosmotropic/chaotropic effect, since the structuring effect of the kosmotropic ions is smaller than expected¹⁴ and direct (water-mediated) interactions of the chaotropic ions on the surface of the biomolecular macromolecule play a crucial role.^{7,15}

Molecular dynamics (MD) simulations of biomolecules in ionic liquid/water mixtures have led to a more detailed picture

(as sketched in Figure 1): Ionic liquid ions with a high charge density, i.e., the ratio between molecular charge and its molecular volume, seem to prefer positions in the vicinity of the oppositely charged amino acids.^{16–19} For example, at low ionic liquid concentrations, trifluoromethanesulfonate CF_3SO_3^- (TRIF, dark blue arrows) preferentially clusters in regions with a positive electrostatic potential.¹⁸ In addition, their mean residence time at these position is much longer than those of ions with low charge density or neutral water molecules.¹⁹ The preference of ions with low charge density, e.g., 1-ethyl-3-methylimidazolium (EMIM, red arrows), for the oppositely charged amino acids is less pronounced. They can also be found in the direct neighborhood of the ionic liquid ions with high charge density (and thus in the vicinity of amino acids with like charge) or even in the proximity of apolar and polar amino acids.^{16–18} The interaction of these ionic liquid ions with the protein surface is less dominated by Coulomb interactions but also influenced by van der Waals interactions of the hydrophobic parts of the ions, e.g., the side chains of imidazolium (tail of the red arrow), with the protein surface. Consequently, their mean residence time at a distinct protein region is shorter,¹⁹ i.e., these ions are more mobile at the protein surface. Nevertheless, the interactions of these ions with low charged density seem crucial for the stability of the protein.¹⁶ Moreover, in hydrated ionic liquid systems, the concentration of ions with low charge density is enriched at the protein surface since their counterions with higher charge density favor the hydration with water molecules in the bulk phase.¹⁸ This may lead to a depletion of water and/or ions with high charge density at the protein surface.^{18,20}

In MD simulations, the stability of the protein correlates with the concentration of the ionic liquid in a bell-shape-like

Special Issue: Wilfred F. van Gunsteren Festschrift

Received: March 7, 2012

Published: June 7, 2012



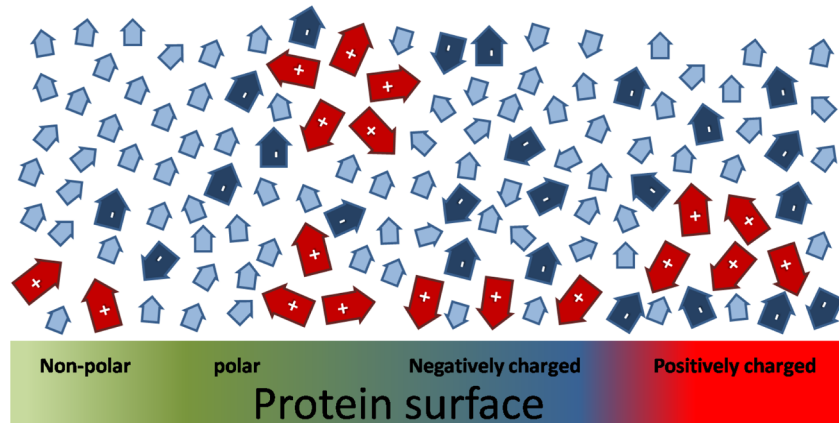


Figure 1. Schematic view of a dissolved protein in a 1-ethyl-3-methylimidazolium (EMIM) trifluoromethanesulfonate (TRIF)/water mixture. The anions (dark blue arrows) possess a high charge density. They prefer the neighborhood of positively charged amino acids or, even more likely, the hydration of water molecules (light blue arrows) in the bulk phase. The cations aggregate in hydrophobic clusters in the bulk phase or are forced to the protein surface.

behavior.^{18,20} With increasing ionic strength of the solution, the Coulomb interactions within the protein stabilize the protein structure.¹⁸ In contrast, the van der Waals interactions within the protein seem to destabilize the protein structure. This results in a bell-shape behavior and shows the transition from a dipolar screening to a charge screening of the solvent molecules at the surface of the protein.¹⁸ At high water mole fractions, the high static dielectric constant of water, $\epsilon(0) \approx 80$, effectively attenuates the Coulomb interactions within the protein. Adding ionic liquid ions to the solution decreases the overall static dielectric constant of the solvent. As a result, attractive Coulomb forces within the protein become stronger, but the van der Waals interaction of the additional hydrophobic ionic liquid cations competes with the van der Waals interaction within the protein, leading to a destabilization of the protein structure.¹⁸ The arrows in Figure 1 indicate that commonly the solvent molecules possess a dipole moment, and consequently their orientation is also determined by the local electric field, resulting in a polarization. The polarization at the surface of the protein is determined by the corresponding local electrostatic potential at the surface and the large dipole moment of the protein itself.

So far, we have discussed the effect of solvent molecules in hydration shells of the protein. In the bulk phase, the hydrophilic anions nitrate (NO_3^-), chloride (Cl^-), acetate (CH_3COO^-), and trifluoromethanesulfonate (CF_3SO_3^-) participate in the hydrogen bond network of the water molecules.^{20–26} Even less hydrophilic anions, e.g., tetrafluoroborate (BF_4^-) and bis(trifluoromethyl)-sulfonyl)amide ($\text{N}-(\text{CF}_3\text{SO}_2)_2^-$), are more or less strongly hydrogen bonded to water molecules.^{21,27–29} In addition to the anion–water hydrogen-bonding, small water clusters to large water networks exist as a function of the water mole fraction.^{22,28,29} Since imidazolium cations seem not to participate in the water–anion network,²⁸ they may form their own clusters.³⁰ The hydrophobic tails aggregate, and the hydrophilic head groups are at the interface with the anions and water (see Figure 1).^{18,23} Additionally, their concentration in the bulk phase may decrease, leading to an enrichment at the protein surface.¹⁸ The transition from the bulk phase to the hydration shells is continuous. Consequently, the dynamics of the solvent molecules change continuously when approaching the protein surface. Since the dynamics and coordination at the protein

surface were analyzed in refs 18 and 19, the present work deals with the dynamics of the solvent molecules in the “bulk phase” and the outer hydration shells.

II. METHODS

Three series of MD simulations of 1-ethyl-3-methylimidazolium (EMIM) trifluoromethanesulfonate (TRIF)/water mixtures with varying water mole fractions $x_{\text{H}_2\text{O}}$ were performed with CHARMM.³¹ The first and second series additionally contain the zinc finger protein SZNF and the protein ubiquitin 1UBQ, respectively. In order to mimic the arrangement of concentric solvation shells, a truncated octahedron was used as a simulation box in these cases. The last series have no solutes and act as a reference system for bulk properties. Therefore, we performed the simulations in a simpler cubic box. An overview of all simulated systems is provided in Table 1. At first glance, a box length between 54.8 and 70.0 Å appears quite large, but a Voronoi analysis reveals the undisturbed formation of four solvation shells only. In other words, all solvent molecules in our simulation systems are members of (maybe distant) solvation shells of the protein and thus do not really mimic the “bulk phase”.

The equilibration of the solvated biomolecules is described in previous studies.^{18,19} For the pure systems, the starting configurations of the systems produced by PACKMOL³² were minimized with the steepest descent method for 200 steps. A first NPT-equilibration covered 1 ns. A second NVT equilibration lasted 0.5 ns with an average edge length of the second half of the initial NPT equilibration. The second NVT equilibration was followed by a production run of about 50 ns at a temperature of 300 K. The respective time step was 2 fs.

The force field parameters of the ionic liquid were taken from Pádua et al.^{33–35} except for the partial charges of the cations, which are given in ref 36. The force field parameter of the biomolecules and water stems from the CHARMM22 force field.³⁷ All bond lengths were kept fixed by a SHAKE algorithm, and long-range electrostatic forces were calculated by a particle-mesh Ewald method with a real-space cutoff of 10 Å and a damping constant κ of 0.41 Å⁻¹.

Table 1. Composition of the 1-Ethyl-3-methylimidazolium (EMIM) Trifluoromethanesulfonate (TRIF)/Water Mixtures Including the Zinc Finger Motif (5ZNF) and Ubiquitin (1UBQ) As a Function of $x_{\text{H}_2\text{O}}$, the Water Mole Fraction^a

including 5ZNF							
$x_{\text{H}_2\text{O}}$	$c_{\text{H}_2\text{O}}$ [mol l^{-1}]	c_{IL} [mol l^{-1}]	#EMIM	#TRIF	# H_2O	d [Å]	ρ_{mass} [g l^{-1}]
1.00	51.8	0.0	0	4	5061	58.6	1022.3
0.93	28.7	2.4	200	204	2557	56.8	1206.8
0.85	19.0	3.4	300	304	1766	57.6	1286.6
0.75	11.8	4.1	312	316	947	54.8	1344.0
0.68	8.8	4.4	345	349	721	55.2	1369.4
including 1UBQ							
$x_{\text{H}_2\text{O}}$	$c_{\text{H}_2\text{O}}$ [mol l^{-1}]	c_{IL} [mol l^{-1}]	#EMIM	#TRIF	# H_2O	d [Å]	ρ_{mass} [g l^{-1}]
1.00	53.6	0.0	0	0	8523	70.01	1019.1
0.88	22.4	3.1	461	461	3366	68.64	1261.6
0.80	15.2	3.8	561	561	2244	68.35	1317.5
0.75	12.1	4.1	592	592	1763	67.90	1339.5
0.66	8.5	4.4	649	649	1244	68.10	1364.9
0.52	5.2	4.7	698	698	768	68.22	1386.4
without solute							
$x_{\text{H}_2\text{O}}$	$c_{\text{H}_2\text{O}}$ [mol l^{-1}]	c_{IL} [mol l^{-1}]	#EMIM	#TRIF	# H_2O	d [Å]	ρ_{mass} [g l^{-1}]
0.97	43.9	1.2	200	200	7428	65.51	1097.8
0.93	32.2	2.3	400	400	5489	65.69	1189.1
0.90	26.2	2.9	500	500	4467	65.66	1235.3
0.85	20.2	3.5	600	600	3444	65.62	1282.2
0.79	14.9	4.1	700	700	2561	65.89	1325.3
0.71	10.7	4.5	770	770	1841	65.95	1352.0
0.65	8.8	4.7	800	800	1504	65.81	1370.8
0.43	3.9	5.1	900	900	678	66.34	1401.5

^a ρ_{mass} and d are the mass density of the system and the edge length of the truncated cuboctahedron, respectively.

III. THEORY

The velocity $v_{i\beta}(t)$ of an atom β in a molecule i can be decomposed into translational, rotational, and vibrational components:

$$v_{i\beta}(t) = v_i^{\text{com}}(t) + \omega_i(t) \times \Delta r_{i\beta}(t) + v_{i\beta}^{\text{vib}}(t) \quad (1)$$

with the distance vector $\Delta r_{i\beta}(t) = \mathbf{r}_{i\beta}(t) - \mathbf{r}_i^{\text{com}}(t)$ pointing from the center-of-mass $\mathbf{r}_i^{\text{com}}(t)$ of the molecule i at time t to the coordinates of the atom β . The velocity of the center-of-mass and the vibrational motion of that atom are denoted by $\mathbf{v}_i^{\text{com}}(t) = d\mathbf{r}_i^{\text{com}}(t)/dt$ and $\mathbf{v}_{i\beta}^{\text{vib}}(t)$, respectively. The last term $\mathbf{v}_{i\beta}^{\text{vib}}(t)$ represents the nonrigidity of the molecule. Since we are interested in the rotational motion of the molecule i , characterized by the angular velocity ω_i , we assume molecule i to be pseudorigid at a first step. In a second step, we will extend our model including the intramolecular vibrations.

A. Pure Rotation of a Rigid Body. The position of the atoms within a rigid molecule can either be given in coordinates of a laboratory coordinate system ($\mathbf{r}_{i\beta}(t) = a_1^{i\beta}(t) \cdot \mathbf{e}_1 + a_2^{i\beta}(t) \cdot \mathbf{e}_2 + a_3^{i\beta}(t) \cdot \mathbf{e}_3$) or in a molecular, body-fixed coordinate system ($\mathbf{r}_{i\beta}(t) = \tilde{a}_1^{i\beta} \mathbf{f}_1(t) + \tilde{a}_2^{i\beta} \mathbf{f}_2(t) + \tilde{a}_3^{i\beta} \mathbf{f}_3(t)$). In the first case, a rotation of the molecule i results in a change of the coordinates $a_i^{i\beta}(t)$,

$a_2^{i\beta}(t)$, and $a_3^{i\beta}(t)$. Since the basis vectors ($\mathbf{e}_1, \mathbf{e}_2, \mathbf{e}_3$) are aligned with the axis of the simulation box, they do not rotate. From the molecular point of view, i.e., the second case, the positions of the atoms within the body-fixed frame of the rigid molecule do not change, but the basis vectors of the body-fixed frame rotate. Consequently, the time behavior of $\mathbf{f}_1^i(t)$, $\mathbf{f}_2^i(t)$, and $\mathbf{f}_3^i(t)$ describes the rotation of the rigid molecule. These vectors are depicted for the cations, anions, water, and biomolecules in Figure 2. In the case of TRIF and water, one of the body-fixed

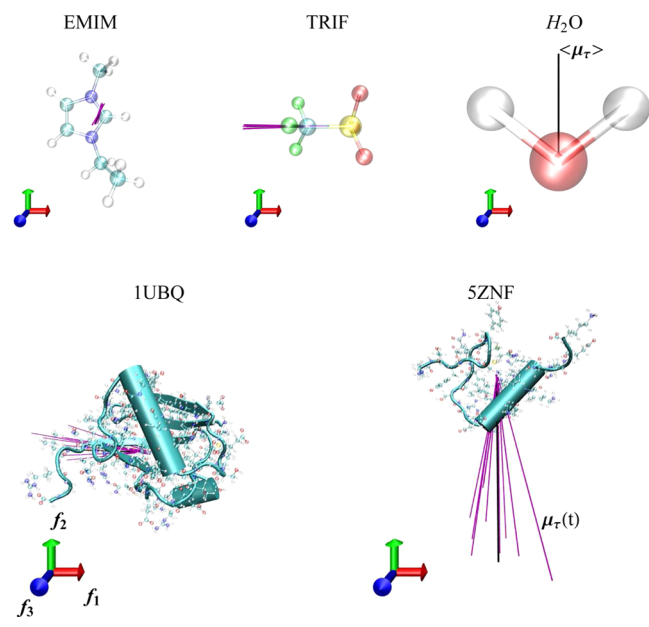


Figure 2. Reference conformations of the three solvent molecules (EMIM, TRIF, and TIP3) as well as the two solutes (5ZNF and 1UBQ). The trihedron defining the body-fixed frame (\mathbf{f}_1 , red; \mathbf{f}_2 , green; \mathbf{f}_3 , blue) is included. Additionally, the mean dipole moment ($\langle \mu \rangle$) for each molecule is given as a black line, and the dipole moment at 10 random time steps ($\mu(t)$) is given in purple.

basis vectors exactly coincides with the dipole moment vector: $\mu_i(t) = -|\mu_i| \mathbf{f}_1^i(t)$ and $\mu_i(t) = |\mu_i| \mathbf{f}_2^i(t)$ for TRIF and water, respectively. In the case of EMIM, the body-fixed frame is orientated with respect to the heterocyclic ring: \mathbf{f}_2 points in the direction of the vector connecting the two nitrogens, and \mathbf{f}_3 is perpendicular to the ring plane. This way, \mathbf{f}_1 points in the direction of the vector connecting C2 and H2, which is also important for the characterization of hydrogen bonding of imidazolium cations. Altogether, the dipole vector $\mu_i(t)$ of EMIM is very close to the body-fixed $\mathbf{f}_2^i(t)$.

The transformation from the laboratory system with the basis vectors $\mathbf{e}_1, \mathbf{e}_2, \mathbf{e}_3$ to the body-fixed system with the basis vectors $\mathbf{f}_1^i(t), \mathbf{f}_2^i(t)$, and $\mathbf{f}_3^i(t)$ can be performed by a Horn algorithm:³⁸

$$(\mathbf{e}_1 \mathbf{e}_2 \mathbf{e}_3) \cdot \begin{pmatrix} a_1^{i\beta}(t) \\ a_2^{i\beta}(t) \\ a_3^{i\beta}(t) \end{pmatrix} = (\mathbf{e}_1 \mathbf{e}_2 \mathbf{e}_3) \cdot (\mathbf{B}^i(t))^T \cdot \mathbf{B}^i(t) \cdot \begin{pmatrix} a_1^{i\beta}(t) \\ a_2^{i\beta}(t) \\ a_3^{i\beta}(t) \end{pmatrix} \quad (2)$$

$$\Rightarrow (\mathbf{f}_1^i(t) \mathbf{f}_2^i(t) \mathbf{f}_3^i(t)) = (\mathbf{e}_1 \mathbf{e}_2 \mathbf{e}_3) \cdot (\mathbf{B}^i(t))^T = (\mathbf{B}^i(t))^T \quad (3)$$

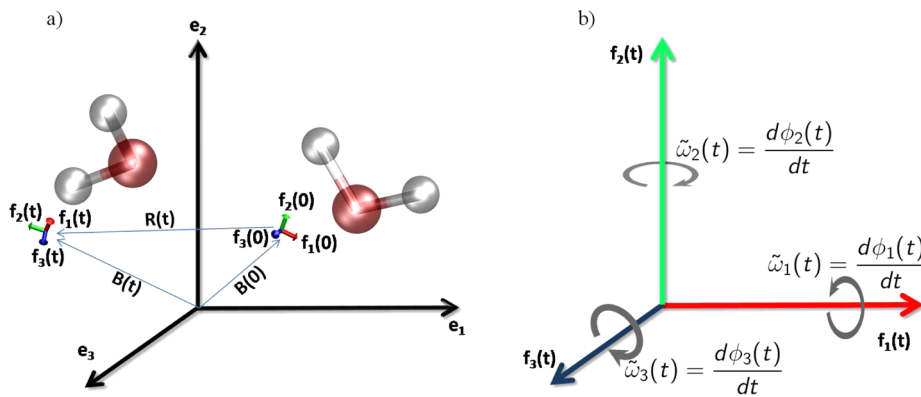


Figure 3. (a) The body-fixed coordinate system with the basis-vectors $\mathbf{f}_1(t)$, $\mathbf{f}_2(t)$, and $\mathbf{f}_3(t)$ can be gained from the coordinates in the laboratory coordinate system by applying the rotation matrix $\mathbf{B}(t)$. The rotation $\mathbf{R}(t)$ of the molecule i during the simulation affects both, laboratory and body-fixed basis vectors. (b) In addition to the rotation of the basis vectors, the atoms of the molecule rotate about the basis vectors. The angular velocities $\tilde{\omega}_1$, $\tilde{\omega}_2$, and $\tilde{\omega}_3$ are the time derivatives of the rotation angles ϕ_1 , ϕ_2 , and ϕ_3 .

$$\Rightarrow \begin{pmatrix} \tilde{\alpha}_1^\beta \\ \tilde{\alpha}_2^\beta \\ \tilde{\alpha}_3^\beta \end{pmatrix} = \mathbf{B}^i(t) \cdot \begin{pmatrix} \alpha_1^{i\beta}(t) \\ \alpha_2^{i\beta}(t) \\ \alpha_3^{i\beta}(t) \end{pmatrix} \quad (4)$$

yielding an orthonormal rotation matrix $\mathbf{B}^i(t)$ for each molecule i in the simulation box, which is equivalent to

$$\mathbf{B}^i(t) = \begin{pmatrix} \mathbf{f}_1^i(t) \\ \mathbf{f}_2^i(t) \\ \mathbf{f}_3^i(t) \end{pmatrix} \quad (5)$$

The rotation of the distance vector $\Delta \mathbf{r}_{i\beta}(t)$ (with respect to the center-of-mass of the rigid molecule i) during the simulation is given by

$$\Delta \mathbf{r}_{i\beta}(t) = \mathbf{R}^i(t) \cdot \Delta \mathbf{r}_{i\beta}(0) \quad (6)$$

with the velocity

$$\mathbf{v}_{i\beta}^{\text{rot}} = \frac{d}{dt} \Delta \mathbf{r}_{i\beta}(t) = \frac{d \mathbf{R}^i(t)}{dt} \cdot \Delta \mathbf{r}_{i\beta}(0) \quad (7)$$

$$= \omega_{i\beta}(t) \times \Delta \mathbf{r}_{i\beta}(t) = \begin{pmatrix} 0 & -\omega_3 & \omega_2 \\ \omega_3 & 0 & -\omega_1 \\ -\omega_2 & \omega_1 & 0 \end{pmatrix} \cdot \Delta \mathbf{r}_{i\beta}(t) \\ = \mathbf{W}^i(t) \cdot \Delta \mathbf{r}_{i\beta}(t) \quad (8)$$

The matrix $\mathbf{W}^i(t)$ of the angular velocity can also be computed by

$$\mathbf{W}^i(t) = \frac{d \mathbf{R}^i(t)}{dt} \cdot (\mathbf{R}^i(t))^T = \frac{d(\mathbf{B}^i(t))^T}{dt} \cdot \mathbf{B}^i(t) \quad (9)$$

using the relationships in eq 3, 6, and 7 and $\mathbf{R}^i(t) = (\mathbf{B}^i(t))^T \cdot \mathbf{B}^i(0)$, which follows from $\mathbf{B}^i(0) \mathbf{f}_k(0) = \mathbf{B}^i(t) \mathbf{f}_k(t) = \mathbf{e}_k$.

The angular velocity vector $\boldsymbol{\omega}_i = (\omega_1, \omega_2, \omega_3)$ can be transformed into the body-fixed frame values $(\tilde{\omega}_1, \tilde{\omega}_2, \tilde{\omega}_3)$ by the matrix $\mathbf{B}^i(t)$ (see eq 4). The meaning of the rotation matrix $\mathbf{R}^i(t)$ and the angular velocity matrix $\mathbf{W}^i(t)$ is illustrated in Figure 3a and b, respectively.

For experimental reasons, the dipole moment vector, $\mu_i(t)$, is an important probe of molecular rotation. It can be also represented as a linear combination of body-fixed axes:

$$\mu_i(t) = \sum_k \tilde{\mu}_k \cdot \mathbf{f}_k(t) \quad (10)$$

The coordinates $\tilde{\mu}_k$ are independent of time for a rigid molecule. Consequently, the dipolar autocorrelation function reads

$$\langle \mu(0) \cdot \mu(t) \rangle = (\tilde{\mu}_1 \mathbf{f}_1(0) \tilde{\mu}_2 \mathbf{f}_2(0) \tilde{\mu}_3 \mathbf{f}_3(0)) \cdot \begin{pmatrix} \tilde{\mu}_1 \mathbf{f}_1(t) \\ \tilde{\mu}_2 \mathbf{f}_2(t) \\ \tilde{\mu}_3 \mathbf{f}_3(t) \end{pmatrix} \\ = \sum_k \sum_l \tilde{\mu}_k \tilde{\mu}_l \langle \mathbf{f}_k(0) \cdot \mathbf{f}_l(t) \rangle \quad (11)$$

$$= \sum_k \sum_l \tilde{\mu}_k \tilde{\mu}_l \langle B_{lk}^i(0) \cdot B_{kl}^i(t) \rangle = \sum_k \sum_l \tilde{\mu}_k \tilde{\mu}_l \langle R_{lk}^i(t) \rangle \quad (12)$$

The matrix product $(\mathbf{B}^i(0))^T \cdot \mathbf{B}^i(t) = (\mathbf{R}^i(t))^T$ representing the inverse of the rotation matrix is called metric. Since no external field is applied to the simulation box and the rotations of the molecules are averages over all members of a species, e.g., all EMIMs in the simulation box, as well as averaged over all time spans t , the matrix $\langle R_{lk}^i(t) \rangle$ approaches zero in the long time limit.

B. Kinematics of a Flexible Body. So far, we have only discussed the pure rotation of rigid molecules, but the present concept can be easily extended to moving and vibrating species as well by introducing time dependent coordinates in the body-fixed frame. Thus, the dipole moments of the previous section may be generalized to those of flexible molecules with dipole coordinates $\tilde{\mu}_1(t)$, $\tilde{\mu}_2(t)$, and $\tilde{\mu}_3(t)$. The velocity and the angular velocity of a flexible, moving particle are given by

$$\mathbf{v}(t) = \sum_k \tilde{v}_k(t) \cdot \mathbf{f}_k(t) \quad (13)$$

$$\boldsymbol{\omega}(t) = \sum_k \tilde{\omega}_k(t) \cdot \mathbf{f}_k(t) \quad (14)$$

The translational D^{trans} and rotational diffusion coefficients D^{rot} can be gained by the integration of the respective autocorrelation functions:

$$D^{\text{trans}} = \frac{1}{3Vk_B T} \int_0^\infty \langle \mathbf{v}(0) \cdot \mathbf{v}(t) \rangle dt = \sum_k \sum_l D_{kl}^{\text{trans}} \quad (15)$$

$$D^{\text{rot}} = \frac{1}{3Vk_B T} \int_0^\infty \langle \boldsymbol{\omega}(0) \cdot \boldsymbol{\omega}(t) \rangle dt = \sum_k \sum_l D_{kl}^{\text{rot}} \quad (16)$$

To a first approximation, the correlation functions in the last two equations, e.g., $\langle \tilde{v}_k(0) \tilde{v}_l(t) R_{lk}(t) \rangle$, may be replaced by the product of single correlation functions, i.e., $\langle \tilde{v}_k(0) \tilde{v}_l(t) \rangle \cdot \langle R_{lk}(t) \rangle$. In a second approximation, one may disregard the relaxation of the metric part since it may relax on a completely different time scale. Moreover, often only diagonal elements of this diffusion coefficient matrix are taken into account. In Table 2, the corresponding diffusion coefficient matrices are gathered.

Table 2. Several Assumptions that Can Be Made In Order to Disentangle the Diffusional Correlations^a

diffusion coefficients	integral of the correlation functions
D_{kl}^{trans}	$\frac{1}{3Vk_B T} \int_0^\infty \langle \tilde{v}_k(0) \tilde{v}_l(t) R_{lk}(t) \rangle dt$
D_{kl}^{rot}	$\frac{1}{3Vk_B T} \int_0^\infty \langle \tilde{\omega}_k(0) \tilde{\omega}_l(t) R_{lk}(t) \rangle dt$
first approximation	
$(1) D_{kl}^{\text{trans}}$	$\frac{1}{3Vk_B T} \int_0^\infty \langle \tilde{v}_k(0) \tilde{v}_l(t) \rangle \cdot \langle R_{lk}(t) \rangle dt$
$(1) D_{kl}^{\text{rot}}$	$\frac{1}{3Vk_B T} \int_0^\infty \langle \tilde{\omega}_k(0) \tilde{\omega}_l(t) \rangle \cdot \langle R_{lk}(t) \rangle dt$
second approximation	
$(2) D_{kl}^{\text{trans}}$	$\frac{1}{3Vk_B T} \int_0^\infty \langle \tilde{v}_k(0) \tilde{v}_l(t) \rangle dt$
$(2) D_{kl}^{\text{rot}}$	$\frac{1}{3Vk_B T} \int_0^\infty \langle \tilde{\omega}_k(0) \tilde{\omega}_l(t) \rangle dt$

^aFurther information is given in the text.

While the relaxation of the metric characterizes the relaxation of the body-fixed axes, the angular velocity autocorrelation function in the body-fixed frame describes rotation about the body-fixed axes. The cumulant expansion developed by Kubo³⁹ provides a relationship between these two types of rotational motion (cf. eq 8 of ref 40):

$$\ln \langle R_{kk}(t) \rangle = - \sum_{l \neq k} \int_0^t \int_0^t \langle \tilde{\omega}_l(t') \tilde{\omega}_l(t'') \rangle dt' dt'' \quad (17)$$

$$= - \sum_{l \neq k} \int_0^t \int_0^t \langle \tilde{\omega}_l(0) \tilde{\omega}_l(s) \rangle ds dt' = -t \sum_{l \neq k} (2) D_{ll}^{\text{rot}}(t) \quad (18)$$

For times t exceeding the relaxation time $\tau_{\tilde{\omega}}$ of the angular velocity correlation function, $(2) D_{ll}^{\text{rot}}(t)$ approaches a constant value such that $\langle R_{kk}(t) \rangle$ decays exponentially with a relaxation time

$$\tau_k = \frac{1}{\sum_{l \neq k} (2) D_{ll}^{\text{rot}}} \quad (19)$$

Integrating the angular velocity and disregarding periodicity

$$\Delta\phi_k(t) = \int_0^t \tilde{\omega}_k(s) ds \quad (20)$$

results in the overall angle covered during rotation until time t .⁴¹ The corresponding mean-squared displacement $\langle \Delta\phi_k^2(t) \rangle$ is the rotational analogue of the translational mean-squared displacement, which correlates with the translational diffusion

coefficient. Correspondingly, it may also be related to the time autocorrelation functions of the respective velocities⁴²

$$\begin{aligned} \langle \Delta\phi_k^2(t) \rangle &= 2t \int_0^t \langle \tilde{\omega}_k(0) \tilde{\omega}_k(s) \rangle ds \\ &\quad - 2 \int_0^t s \cdot \langle \tilde{\omega}_k(0) \tilde{\omega}_k(s) \rangle ds \end{aligned} \quad (21)$$

After a sufficiently long time, both integrals in the last equation reach constant values. As a result, $\langle \Delta\phi_k^2(t) \rangle$ becomes linear. Its slope in this time regime yields the rotational diffusion coefficient for each axis k :

$$(2) D_{kk}^{\text{rot}} = \frac{1}{2} \lim_{t \rightarrow \infty} \frac{d}{dt} \langle \Delta\phi_k^2(t) \rangle = \int_0^t \langle \tilde{\omega}_k(0) \tilde{\omega}_k(s) \rangle ds \quad (22)$$

These diffusion coefficients are correlated with the respective relaxation time constants τ_k via eq 19.

IV. RESULTS AND DISCUSSION

A. Structural Packing. The structure in pure ionic liquids is commonly characterized by charge ordering with alternating layers of cations and anions. Adding water to this liquid will disrupt the cation–anion network. This can be easily shown by the radial distribution functions (RDF) with respect to the centers of mass,⁴³ $g_{\text{EMIM-EMIM}}^{000}(r)$, $g_{\text{TRIF-TRIF}}^{000}(r)$, and $g_{\text{EMIM-TRIF}}^{000}(r)$, depicted in the first row of Figure 4. The overall cation–anion network is characterized by the charge ordering function:

$$Q(r) = g_{\text{EMIM-EMIM}}^{000}(r) + g_{\text{TRIF-TRIF}}^{000}(r) - 2g_{\text{EMIM-TRIF}}^{000}(r) \quad (23)$$

which is shown in Figure 5 as a function of water mole fraction $x_{\text{H}_2\text{O}}$. It can be represented for each $x_{\text{H}_2\text{O}}$ by a fit function⁴¹

$$Q_{\text{fit}}(r) = \frac{A}{r} e^{-r/\sigma} \sin\left(\frac{2\pi r}{\lambda} + \phi\right) \quad (24)$$

in the distance range from $r_{\min} = 4 \text{ \AA}$ to $r_{\max} = 30 \text{ \AA}$ with a constant phase shift of $\phi = 24.82$. The corresponding fit parameters are given in Table 3. Quite intuitively, the damping factor $1/\sigma$ and the “wave length” λ increase monotonically with increasing $x_{\text{H}_2\text{O}}$, showing the dielectric screening effect of the interstitial water dipoles on the electrostatic forces between the ions. The increasing λ values indicate a broadening of the charge layers, i.e., the emerging hydration of the ions. This screening effect is also clearly visible in $g_{\text{TRIF-TRIF}}^{000}(r)$ and $g_{\text{EMIM-TRIF}}^{000}(r)$. Simultaneously, weaker repulsion between anions leads to a slight shift to shorter distances, whereas the weaker attraction between cation and anion results in a slight shift toward longer distances. This was also observed for EMIM acetate.²⁶

The emerging interaction of the ions with water is shown in the bottom row of Figure 4. We find extremely high first peaks at $x_{\text{H}_2\text{O}} = 0.43$ with values of more than 3.0 and even more than 7.0 in the case of anion–water and water–water aggregation, indicating a strong anion–water network at high ionic strength. As the rather bulky cations do not fit into this network, they are expelled to alternative regions of space. Thus, they get closer to each other explaining the short cation–cation distances at $x_{\text{H}_2\text{O}} = 0.43$. This may be also indicative of nanostructured regions in ILs already reported in the literature.³⁰

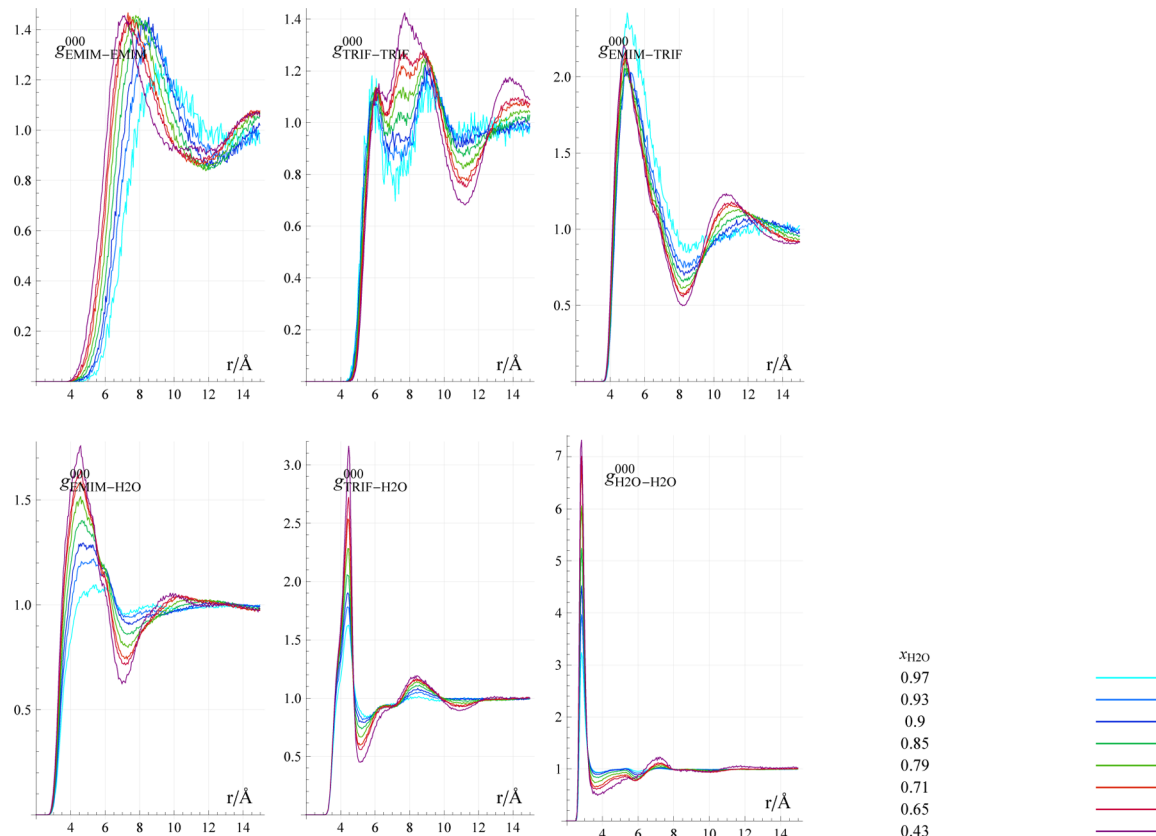


Figure 4. $g^{000}(r)$ for all solvent species combinations in the ionic liquid/water systems without solute.

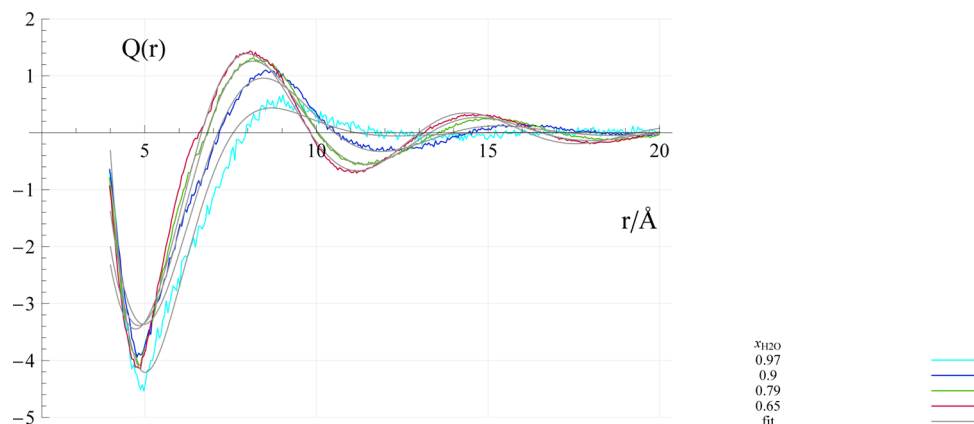


Figure 5. Charge ordering function $Q(r)$ and fits (see Table 3 for parameter values) for selected water mole fractions of ionic liquid/water systems without solute.

Table 3. Fitted Parameters of the Charge Ordering Function $Q_{\text{fit}}(r)$ in the Hydrated Ionic Liquid Systems without a Biomolecular Solute

$x_{\text{H}_2\text{O}}$	amplitude A	damping factor $1/\sigma$	wavelength λ
0.43	28.08	0.11	6.23
0.65	31.35	0.13	6.34
0.71	32.11	0.13	6.38
0.79	35.53	0.15	6.49
0.85	41.23	0.17	6.64
0.90	53.96	0.22	6.80
0.93	81.71	0.28	6.97
0.97	294.4	0.48	7.22

It seems that the effect of the penetrating water molecules on the ionic network structure is strongest in the case of $g_{\text{TRIF-TRIF}}^{000}(r)$. With increasing water concentration, the broad peak around 7.5 Å can be deconvoluted into two peaks with maxima at roughly 6 and 9 Å. Since two solvation shells may contribute to the broad peak at 7.5 Å, a discussion solely on the basis of radial distribution functions is inappropriate for these anisotropic molecules.²⁹ Decomposing the radial distribution function $g_{\text{TRIF-TRIF}}^{000}$ at $x_{\text{H}_2\text{O}} = 0.43$ and 0.97 in Figure 4 by means of Voronoi tessellation shows indeed that the broad peak is a superposition of the first and second solvation shell of TRIF around TRIF. At low water concentrations, the first shell of TRIF (red line) and the second shell of TRIF (orange line) overlap. Increasing water concentration shifts the center of both

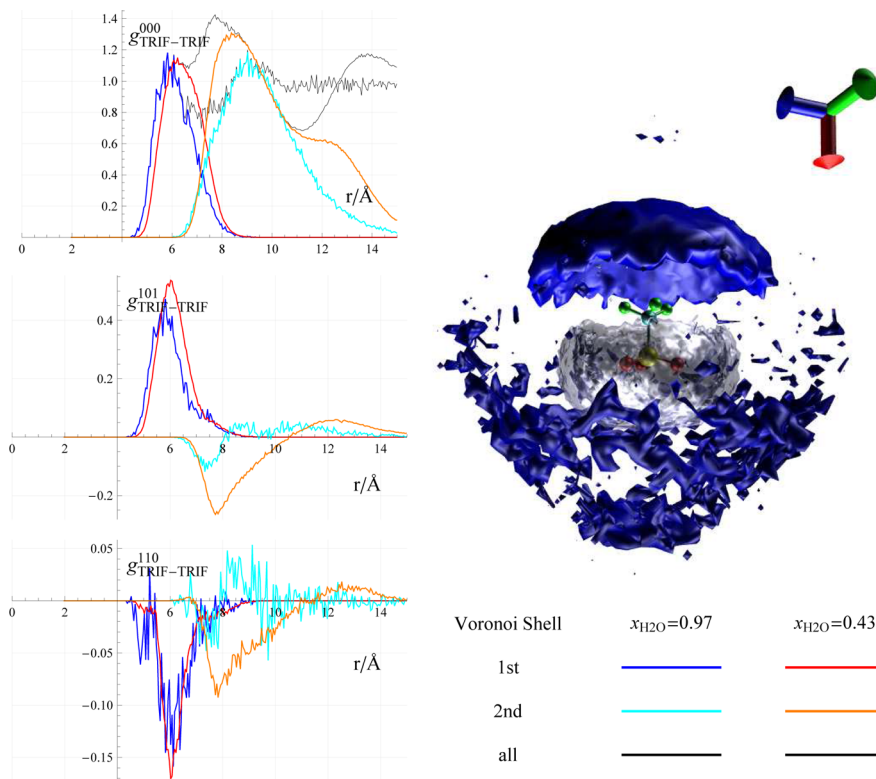


Figure 6. Decomposition of radial ($g^{000}(r)$) and orientational correlation functions, $g^{101}(r)$ and $g^{110}(r)$ for TRIF around TRIF into Voronoi solvation shells. $g^{101}(r)$ characterizes the mutual orientation of molecules, whereas $g^{110}(r)$ probes the alignment of dipoles at a certain distance. Surrounding TRIF and H_2O in the 3D density plot are represented by dark blue and gray surfaces, respectively.

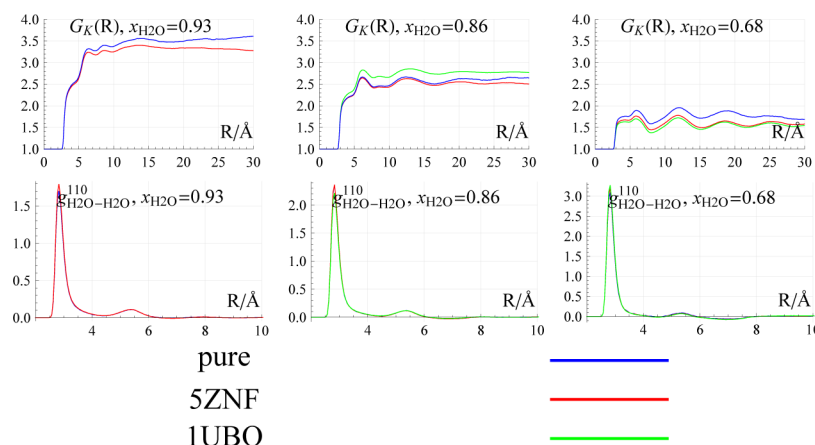


Figure 7. R-dependent $G_k(R)$ factor (upper row) and the dipole–dipole spatial correlation function (lower row), $g^{110}(r)$, for water in the three systems: pure ionic liquid/water mixtures and including the biomolecules 5ZNF and 1UBQ as a function of the water mole fraction.

solvation shells in different directions: The first solvation shell shifts to shorter distances (blue line), whereas the second solvation shell resides now at 9 Å for $x_{\text{H}_2\text{O}} = 0.97$ caused by the intruding water molecules. As a result, the shape of the second peak changes drastically. Since TRIF in the first solvation shell of the reference triflate is a direct neighbor of the central TRIF, the influence of the water molecules can only be of an indirect nature. Consequently, the shape of the first peak changes much less. This is also seen in the mutual orientation of the triflates around themselves measured by $g^{101}(r)$ and $g^{202}(r)$.^{43,44} In the first shell, the values of $g^{101}(r)$ are positive; i.e., the dipole of the reference TRIF and the vector connecting the center of mass of the reference molecule with the neighboring TRIF is less than

90°. The preferred positions of these triflates are visible as a dark blue region in the proximity of the CF_3 group in Figure 6 since the dipole vector of the reference triflate points in the opposite direction of the red f_1 axis, i.e., from the sulfonyl group toward the CF_3 group.

The second shell of $g_{\text{TRIF-TRIF}}^{101}(r)$ (orange line) shows negative values at $x_{\text{H}_2\text{O}} = 0.43$. Consequently, the triflate in the second shell can be found closer to the sulfonyl group (tattered blue region at the bottom of Figure 6). In between, the first shell of water molecules (white region) damps the repulsion between the triflates. With increasing water content, the preference for a distinct position of the neighboring triflate around the central triflate decreases. This goes along with a

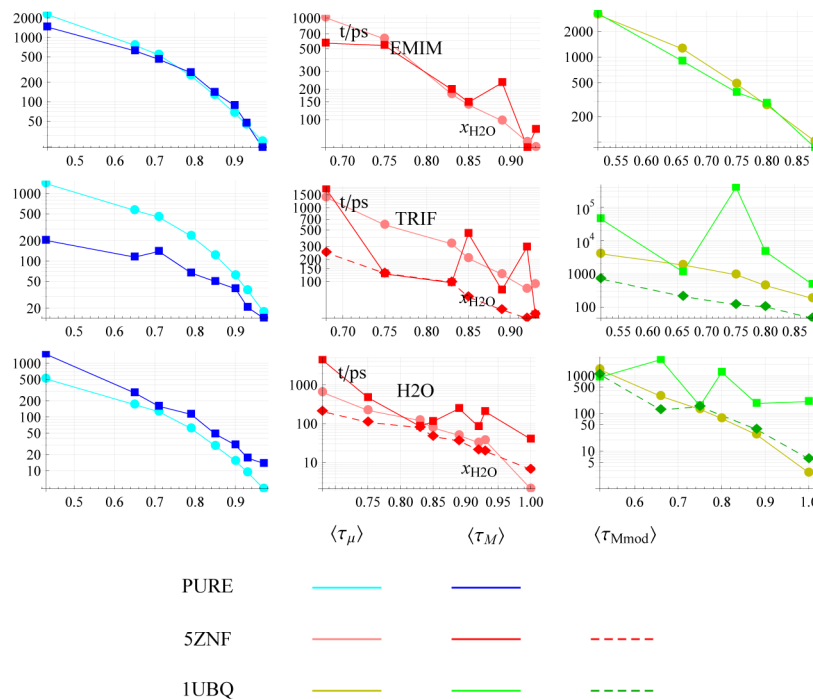


Figure 8. Average relaxation times of the single molecule dipole moment $\langle \tau_\mu \rangle$ and of the collective dipole moment $\langle \tau_M \rangle$, as well as the modified collective dipole moment relaxation times $\langle \tau_{M\text{mod}} \rangle$ without the long time constants.

weaker alignment of anionic dipoles. At low water content ($x_{\text{H}_2\text{O}} = 0.43$), both first shell (red) and second shell (orange) anionic dipole moments prefer a more or less antiparallel alignment indicated by the negative values of $g^{110}(r)$; i.e., the angle between these dipoles is greater than 90° . At high water content, the first shell keeps its antiparallel alignment, whereas the second shell (light blue) shows no systematic alignment any more.

B. Correlation between Structure and Dynamics. In principle, the ionic network in ionic liquids is of a collective nature. In order to characterize the collective dipole–dipole interactions, one may integrate the orientational correlation function $g^{110}(r)$

$$G_k(R) = 1 + \frac{N}{V} \int_0^R g^{110}(r) 4\pi r^2 dr \quad (25)$$

$$= \frac{1}{N} \sum_i \sum_j \left\langle \frac{\boldsymbol{\mu}_i \cdot \boldsymbol{\mu}_j}{|\boldsymbol{\mu}_i| |\boldsymbol{\mu}_j|} \right\rangle \quad (26)$$

in order to obtain the distance dependent Kirkwood factor $G_k(R)$.^{44–46} Figure 7 shows $G_k(R)$ as a running integral of the dipolar $g^{110}(r)$ for three selected mole fractions $x_{\text{H}_2\text{O}}$, with and without a biomolecular solute. At low $x_{\text{H}_2\text{O}}$, the orientation of the water dipoles is very strong. Increasing the water content, the Kirkwood factor increases from roughly 1.5 to 3.5, although the maximum of the corresponding $g^{110}(r)$ drops from 3.3 to 1.8. It seems that the weakening of the mutual water–water orientation is compensated by the increasing number of water–water interactions. Additionally, antiparallel alignments of water dipoles at longer distances, e.g., between 6 and 8 Å at $x_{\text{H}_2\text{O}} = 0.68$, disappear at higher water mole fractions, thus increasing the value of $G_k(R)$. However, the biomolecule seems to have

little influence on the mutual orientation of the water molecules.

The values of the $g^{110}(r)$ of imidazolium cations in the solvation shells are an order of magnitude smaller compared to the corresponding $g_{\text{H}_2\text{O}-\text{H}_2\text{O}}^{110}(r)$ due to the weaker interaction and larger anisotropy of the cations. Consequently, the computation of the $g_{\text{EMIM}-\text{EMIM}}^{110}(r)$ on the basis of eq 25 is tedious because of the r^2 -amplified noise of $g_{\text{EMIM}-\text{EMIM}}^{110}(r)$ at longer distances. The long-distance limit of $G_k(R)$ equals $\langle (\sum \boldsymbol{\mu}_i)^2 \rangle / (N(\boldsymbol{\mu})^2)$, which can be easily deduced from eq 26. As a result, the Kirkwood G_k factors for EMIM and TRIF are 1.00 and 0.33, respectively.

The G_k factor as a measure of collective orientational structure enables a transition from single particle dynamics to collective dynamics via the Kievelson–Madden relation⁴⁷

$$\langle \tau_M \rangle = G_k \cdot \langle \tau_\mu \rangle \quad (27)$$

which connects the relaxation time $\langle \tau_M \rangle$ of the collective dipole moment $\mathbf{M} = \sum \boldsymbol{\mu}_i$ with that of the single molecule dipole moment $\langle \tau_\mu \rangle$. The three molecular species, EMIM, TRIF, and H₂O, represent all three possibilities: As G_k is close to one for EMIM, $\langle \tau_M \rangle$ and $\langle \tau_\mu \rangle$ should be equal. As can be seen from the first row of Figure 8, this is fairly valid for the pure system as well as for the two protein solutes. The only two exceptions are at mole fractions $x_{\text{H}_2\text{O}} = 0.89$ and 0.68 in the SZNF system. For TRIF, collective relaxation should be faster (!) than single dipole relaxation, a rather unexpected behavior. This is indeed the case as is visible in the second row of Figure 8 for the ionic liquid/water mixture without biomolecules.

However, the ratio $\langle \tau_M \rangle / \langle \tau_\mu \rangle$ is not constant but increases with increasing ionic strength. For two protein systems, SZNF and 1UBQ, the underlying multiexponential model of relaxation produces some peculiarities. The problem is caused by TRIF molecules which undergo a tight binding to the protein, resulting in a high relaxation time.¹⁹ Therefore, we

Table 4. Fitting Parameter of the Logistic Functions (see eq 28) Which Represent the Reciprocal Diffusion Coefficients $1/D^{\text{trans}}$ and Rotational Relaxation Times $\langle\tau\rangle$ of the Molecular Species As a Function of Water Mole Fraction

	$1/D^{\text{trans}} [6 \times 10^4 \text{ cm}^{-2} \text{ s}]$				$\langle\tau_\mu\rangle [10^{-12} \text{ s}]$			
	a_0	a	k	x_I	a_0	a	k	x_I
without solute								
H_2O	-1.24	44.68	8.63	0.58	H_2O	0.00	682.8	9.75
TRIF	-6.71	336.4	9.34	0.55	TRIF	0.00	1729.	9.51
EMIM	-7.75	275.6	7.98	0.54	EMIM	0.00	2981.	9.92
SZNF	$1/D^{\text{trans}} [6 \times 10^4 \text{ cm}^{-2} \text{ s}]$				$\langle\tau_\mu\rangle [10^{-12} \text{ s}]$			
including SZNF	a_0	a	k	x_I	a_0	a	k	x_I
H_2O	-0.41	51.40	11.27	0.61	H_2O	0.00	1500.	13.00
TRIF	0.16	207.8	17.63	0.70	TRIF	27.4	2002.	16.43
EMIM	0.00	124.8	18.50	0.73	EMIM	0.10	2100.	15.00
SZNF	4.65	3377.	20.57	0.72	SZNF	1000.	1.0×10^6	20.00
including 1UBQ	$1/D^{\text{trans}} [6 \times 10^4 \text{ cm}^{-2} \text{ s}]$				$\langle\tau_\mu\rangle [10^{-12} \text{ s}]$			
1UBQ	a_0	a	k	x_I	a_0	a	k	x_I
H_2O	0.00	51.38	11.17	0.60	H_2O	-4.48	3365.	11.05
TRIF	0.00	629.3	12.72	0.56	TRIF	0.00	5499.	11.55
EMIM	0.00	316.2	12.29	0.60	EMIM	4.87	4472.	12.96
1UBQ	40.1	9178.	17.14	0.60	1UBQ	2400	2.1×10^6	15.00

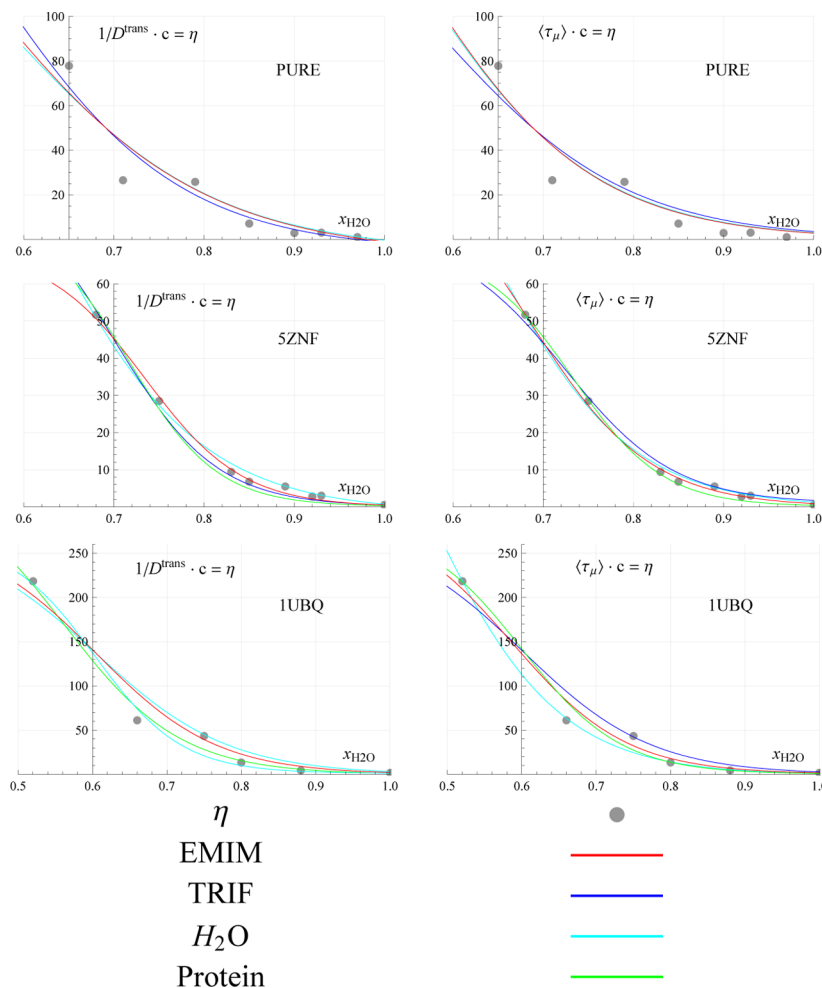


Figure 9. Logistic fits of the reciprocal diffusion coefficient, $1/D^{\text{trans}}$, and the average reorientation times $\langle\tau_\mu\rangle$ for the three solvent species, EMIM, TRIF, and H_2O , and the two biomolecular solutes, SZNF and 1UBQ, scaled by a factor c to coincide with the viscosities.

have tried to remove the longest relaxation time from the multiexponential fit. The resulting $\langle\tau_M^{\text{mod}}\rangle$'s are represented by dashed lines in Figure 8. Of course, this reduces the average collective relaxation time, but the remnant value now scales

with the single particle relaxation time. The respective ratio seems to be constant as a function of the mole fraction, proving the viscosity scaling discussed later. For water, collective relaxation should be slower than single particle reorientation as

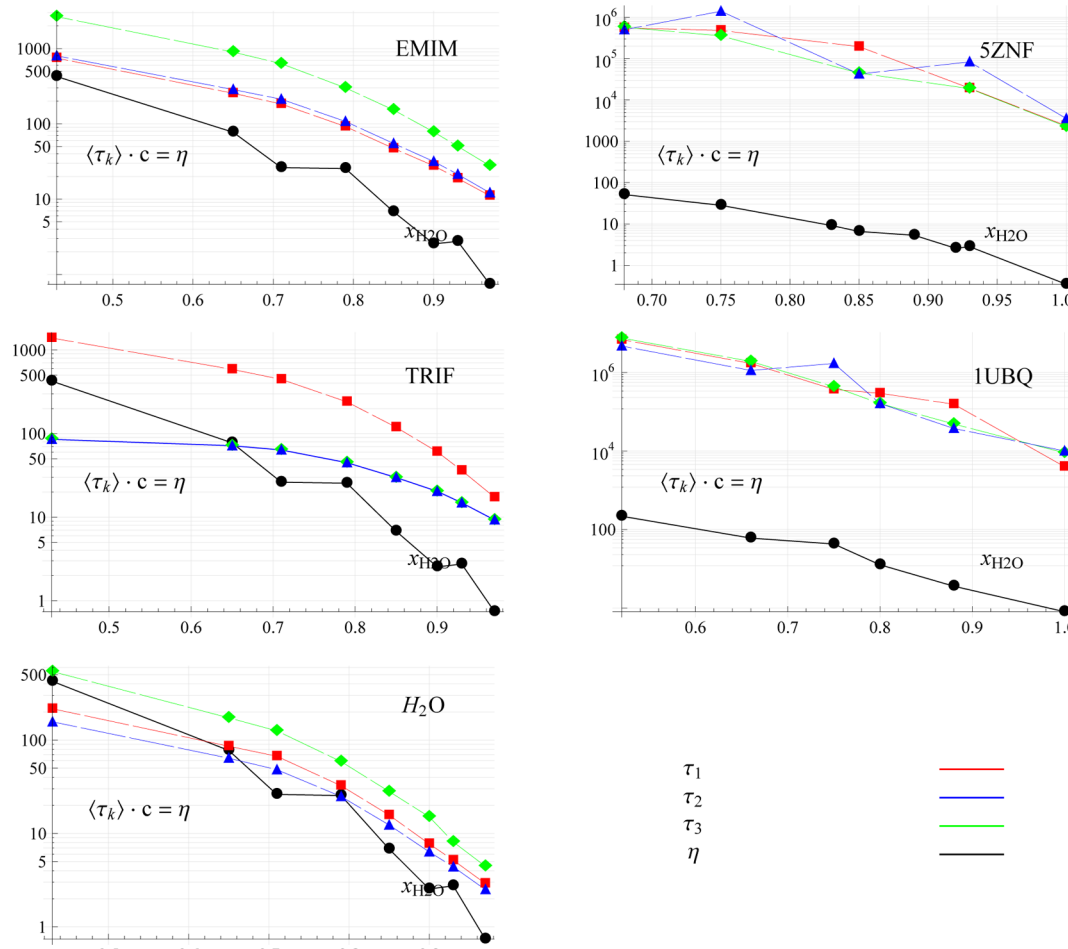


Figure 10. Average relaxation times, $\langle \tau_k \rangle$ (in ps), of the diagonal terms of the metric, $\langle R_{kk}(t) \rangle$, and viscosities, η (in mPa s). The values for the solvent species (EMIM, TRIF, and H₂O) correspond to the simulation of the ionic liquid/water mixtures without a biomolecule.

visible in the third row of Figure 8. Without a biomolecule, the ratio $\langle \tau_M \rangle / \langle \tau_\mu \rangle$ resembles the behavior of the G_k factor although reduced by a factor of two-thirds. Water molecules solvating protein solutes again produce peculiarities which make it difficult to identify a clear-cut ratio. Elimination of the long time constants in the multiexponential model, as already done for TRIF, also results in a fairly constant ratio, and $\langle \tau_M^{\text{mod}} \rangle$ again obeys viscosity scaling. The respective modified G_k factor, however, is around unity.

C. Single Particle Dynamics in the Laboratory Frame.

The structural changes with increasing water content affect the dynamics of the solvent molecules as well. The diffusion of the solvent molecules is increased, and their rotation is enhanced. In fact, the trend for each molecular species in the three simulation systems (without solute, including 5ZNF or 1UBQ) can be fitted by a logistic function

$$f(x_{H_2O}) = a_0 + \frac{a}{1 + e^{-k(x_{H_2O} - x_i)}} \quad (28)$$

with the parameters given in Table 4. We note that these fits are restricted to the range of our simulated x_{H_2O} and should not be used for extrapolation outside this range.

The logistic functions drop monotonically from $a_0 + a$ to a_0 with an inflection point at x_i . The slope is determined by the parameter k , which measures the influence of the ionic strength. Interestingly, the biomolecular solute seems to act as an

effective enhancement of the ionic strength since its influence increases in the following order: without biomolecule < including 1UBQ < including 5ZNF. The trend for the inflection point is in the opposite direction; i.e., it reaches the lowest value for the systems without a solute.

However, the viscosity of the systems follows a slightly different trend: without biomolecule < including 5ZNF < including 1UBQ. Nevertheless, a viscosity scaling can be observed for all systems as visible in Figure 9: $\eta = cf(x_{H_2O})$. The constant c was obtained by a least-squares fit of $cf(x)$ to the viscosity values. From a theoretical point of view, the viscosity scaling can be interpreted in terms of hydrodynamic relations⁴⁸

$$\frac{1}{D^{\text{trans}}} = \frac{6\pi r}{k_B T} \eta \quad (29)$$

$$\frac{1}{D^{\text{rot}}} = \frac{8\pi r^3}{k_B T} \eta \simeq \langle \tau_\mu \rangle \quad (30)$$

which involve the shear viscosity η and the hydrodynamic radius r . This way, the constants c may be converted to hydrodynamic radii, but the so-obtained values are far from realistic values, as expected from previous studies.²⁸ For example, the radius of the solvent molecules would be a quarter of their maximum intramolecular distance. On the contrary, the radius of the protein equals 4 times the maximum distance.

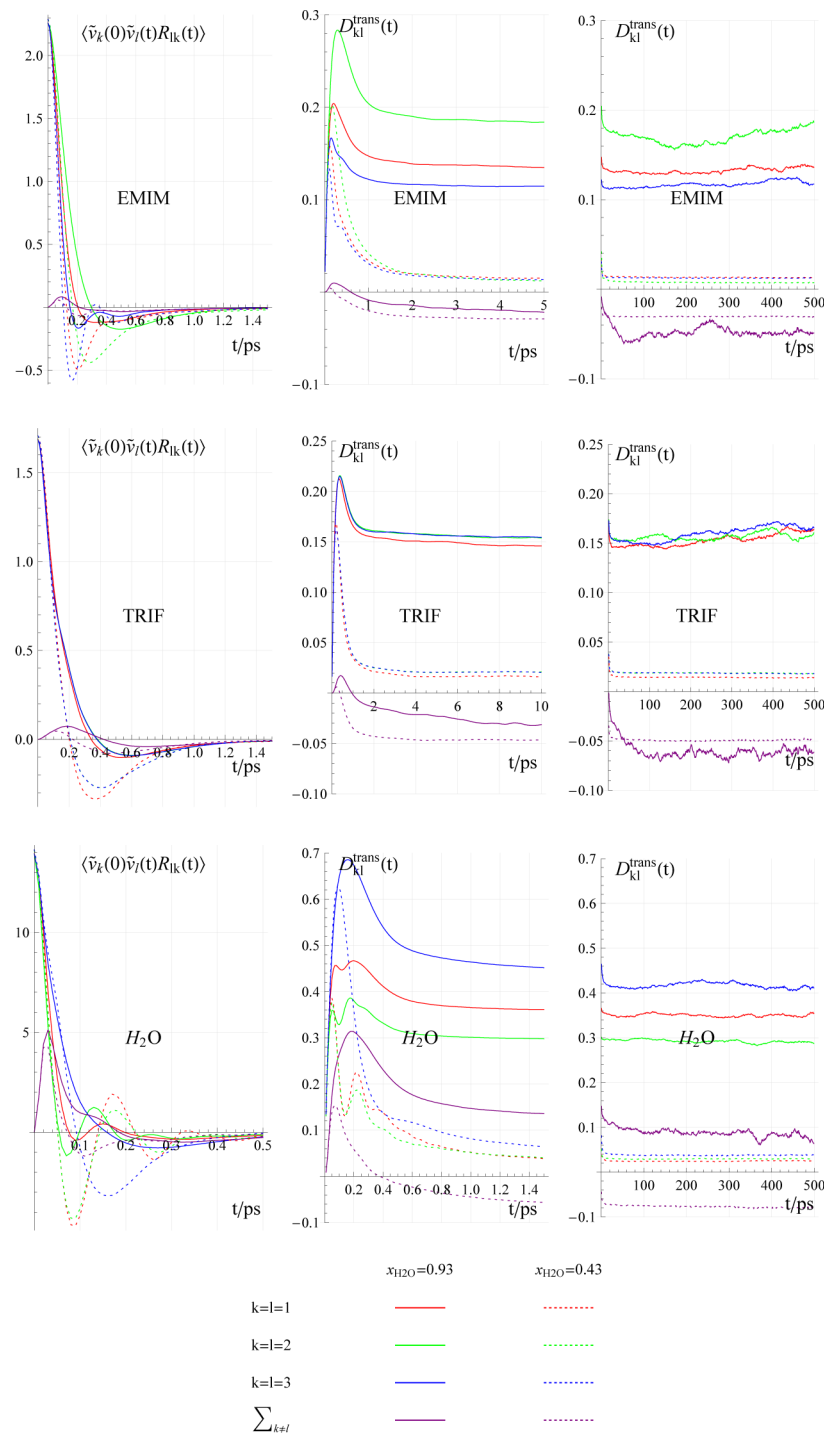


Figure 11. Left column: translational velocity autocorrelation function, decomposed into diagonal terms ($k = l = 1, 2, 3$) and the sum of off-diagonal terms ($k \neq l$). Middle and right column: Integral of the translational velocity autocorrelation function, short-term and long-term behavior.

So far, reorientation in the laboratory frame was restricted to a single body-fixed axis, the dipole moment vector μ . The inherent anisotropy of molecular ions, however, requires a description of reorientation in terms of all three body-fixed axes, in other words, the relaxation of the metric $R_{lk}(t)$. Fitting the diagonal terms of the metric, $\langle R_{kk}(t) \rangle$, again multi-exponentially, yields the average relaxation times, $\langle \tau_k \rangle$, as a function of the mole fraction, as shown in Figure 10.

For the pure systems, the three solvent species exhibit the following behavior: TRIF and EMIM appear—in a dynamical sense—as rotational prolate ellipsoids with the axis coinciding

with the dipole moment vector being the major axis. The rotational dynamics of water resembles that of a general ellipsoid with three different relaxation times. It is interesting to note that for all three solvent species only the major axis, i.e., the dipole axis, obeys viscosity scaling, as shown above in Figure 9. In fact, the two minor axes depend on the ionic strength to a lesser extent as compared to the viscosity. The rotational dynamics of the two proteins, 5ZNF and 1UBQ, seems to be that of a spherical top (Figure 10) within the statistical accuracy achievable in a 200 ns simulation.

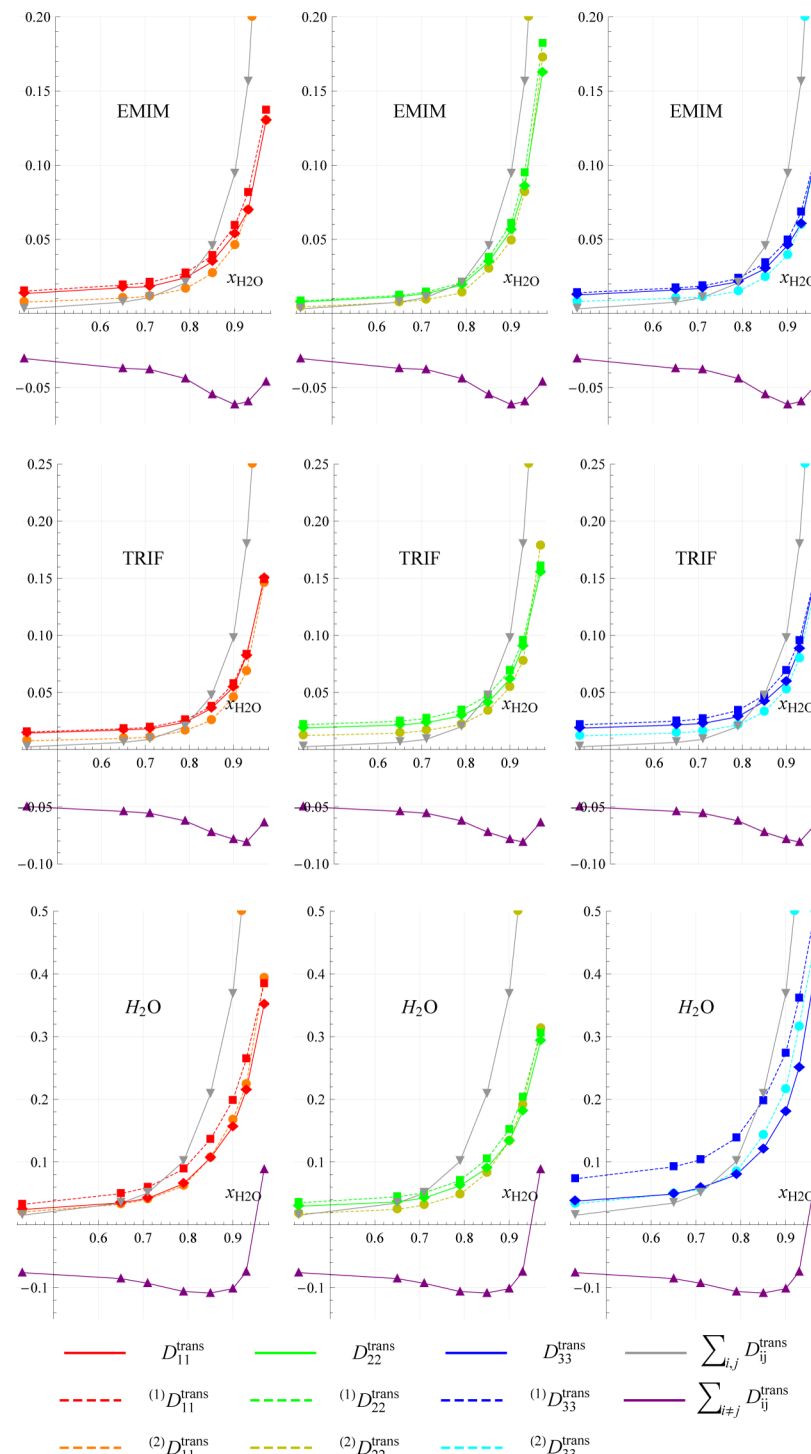


Figure 12. Partial translational diffusion coefficients (diffusion tensor elements), D_{kk}^{trans} , and approximations, $(1)D_{kk}^{\text{trans}}$ and $(2)D_{kk}^{\text{trans}}$, as well as the sum of the off-diagonal elements and the total sum, the translational diffusion coefficient (times three).

D. Single Particle Dynamics in the Body Fixed Frame. Anisotropy of shape and charge distribution is a genuine feature of molecular ionic liquids and the ultimate reason for their liquidity at room temperature. Of course, this anisotropy is also reflected in the static structure, but dynamics is usually much more sensitive to the interactions between molecules. Therefore, we will resolve the anisotropic character of translational and rotational dynamics of solvent species in full detail. The dynamics of the biomolecular solutes is given in the Supporting Information. In both cases, we switch from a description in the

laboratory frame to the projection of dynamics to body-fixed axes.

1. Decomposition of Translational Motion. Figure 11 displays the decomposition of the translational velocity autocorrelation function, $\langle \vec{v}(0) \cdot \vec{v}(t) \rangle$ (left column), and the respective diffusion coefficient, D^{trans} (middle and right column), for the solvent molecules. For the highest and lowest mole fraction, a set of four curves is given, including the three diagonal terms colored in accordance with the definition of body-fixed axes in Figure 2. The fourth component is the sum

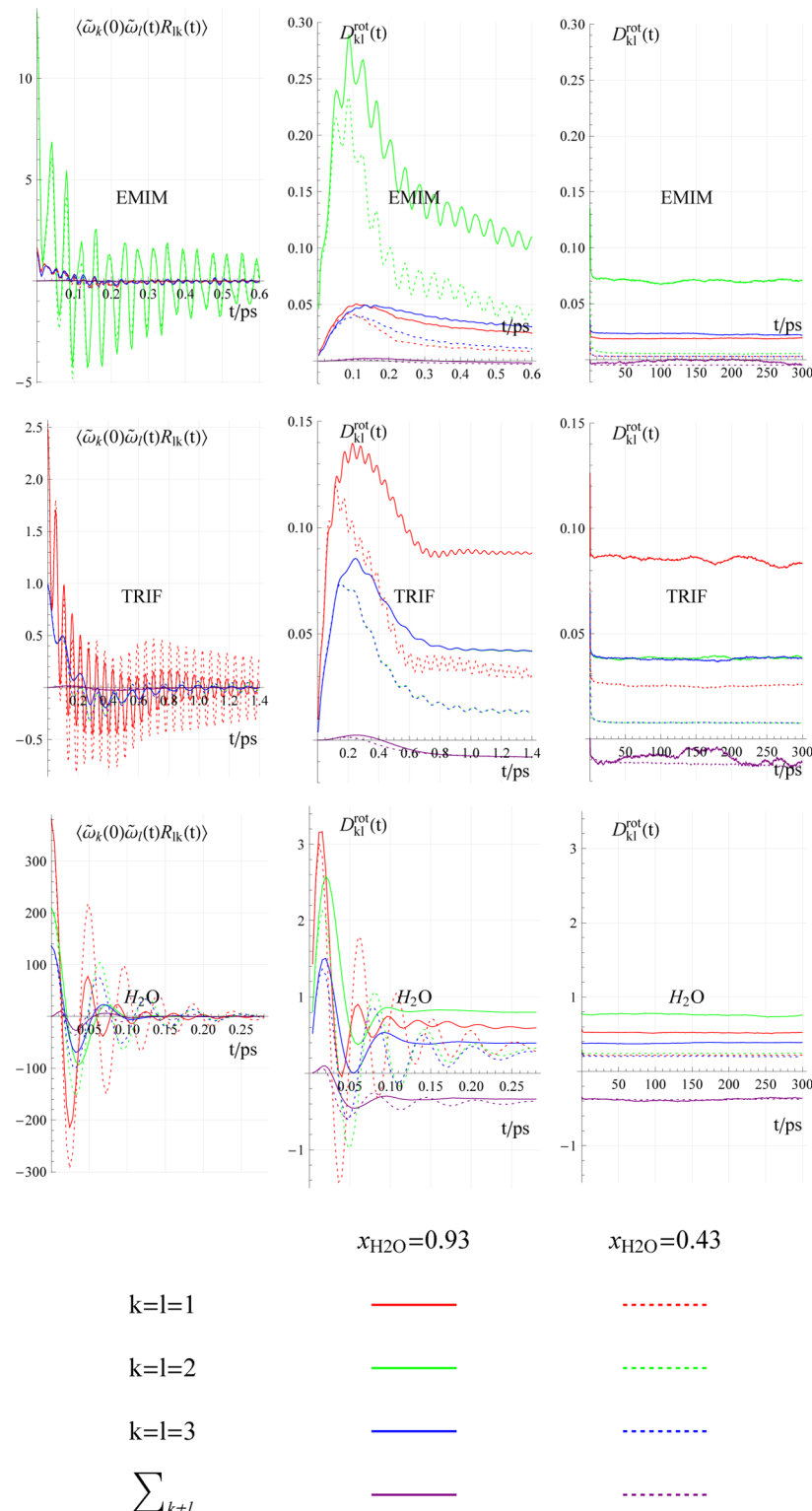


Figure 13. Left column: angular velocity autocorrelation function, decomposed into diagonal terms ($k = l = 1, 2, 3$) and the sum of off-diagonal terms ($k \neq l$). Middle and right column: Integral of the angular velocity autocorrelation function, short-time and long-time behavior.

of all nondiagonal elements $\sum_k \sum_l D_{kl}^{\text{trans}}$. Comparing the lowest and highest ionic strength, a dramatic change of the decomposed translational motion (see first column in Figure 11) can be observed. For all components of the velocity correlation function, their first minimum steps down at high ionic strength and shifts to shorter times. This shift can be clearly seen in the respective power spectra (data not shown).

It can be interpreted as an enhanced backward motion, or rebound, of a molecule trapped in a cage built up by its neighbors following the initial forward movement along a preferred body-fixed axis. The elevated frequency of this “rattling the cage”⁴⁹ is caused by the stronger electrostatic forces at high ionic strength.

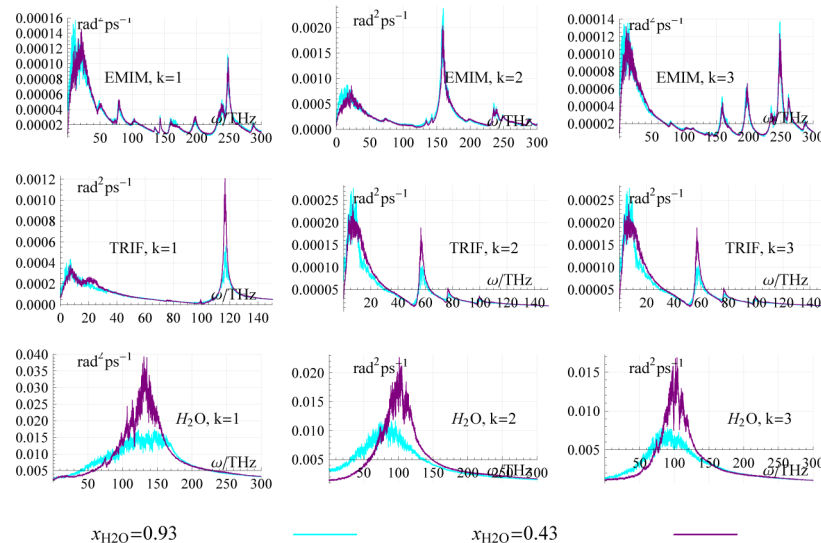


Figure 14. Power spectra of the rotational angular velocity autocorrelation functions.

The molecular structure of TRIF suggests that diffusion along the C-S axis ($-f_1$ axis = dipole moment axis and axis of minimum moment of inertia, c.f. Figure 2) is accelerated as compared to the two (equivalent) perpendicular axes. The higher oscillatory character, i.e., the deeper negative region in the respective velocity component correlation function, however, leads to a smaller partial diffusion coefficient (cf. right column in Figure 10, D_{11}^{trans} is smaller than D_{22}^{trans} and D_{33}^{trans}). For EMIM, a more subtle behavior is observed: At low ionic strength, it is intuitive; i.e., diffusion is faster along the axis of minimum moment of inertia (f_2 = close to the dipole moment axis), but it is counterintuitive, i.e., slower, at high ionic strength (right column in Figure 11).

At first glance, these running integrals of the solvent diffusion coefficients seem to converge on a time scale of several picoseconds (middle column of Figure 11). However, it turns out that the final values are reached in an asymptotic time regime up to 0.5 ns for solvent molecules and solutes (see Supporting Information). In fact, we took the final values of the partial diffusion coefficients (Figure 12) from the average in the time window 0.1 to 0.3 ns. This demonstrates once more the highly compensatory character of correlations in ionic liquids which almost annihilate each other upon integration, leading to a very small final value. A most prominent example is the low conductivity of ionic liquids.⁵⁰

The almost perfect compensation of positive and negative contributions upon integration is not limited to contributions of a single diagonal or off-diagonal components but applies to a mutual compensation between diagonal and off-diagonal components as well. In contrast to the running integrals of the diagonal elements, the sum of off-diagonal terms converge on a time scale of several picoseconds. The sum of the converged off-diagonal values are of comparable size to the sum of the diagonal terms. Quite generally, the sum of off-diagonal elements decreases the overall diffusion coefficient with the single exception of water at a high water mole fraction (Figure 12). As a result, the overall diffusion coefficient is further reduced according to the increased importance of the off-diagonal terms. As they describe the cross correlation between different axes, an increase of their relative importance implies an increased translational hampering along preferred axes. While, at low ionic strength, translation along different axes is

almost free or slightly coupled, at high ionic strength, translation along one axis immediately induces translation along other axes such that the net or overall displacement is quite modest. This trend should be at the maximum for the pure ionic liquid.

The previous analysis is based on the full correlation functions simultaneously considering the body-fixed coordinates and the metric $R_{kk}(t)$. Comparing the time scales in Figure 10 with that of Figure 11, which differ by at least 2 orders of magnitude, it might be tempting to consider the correlation functions of the body-fixed coordinates alone, leaving aside the metric (see second approximation of Table 2). Unfortunately, these diagonal diffusion coefficients ${}^{(2)}D_{kk}^{\text{trans}}$ computed from the body-fixed velocity coordinates only underestimate the diagonal diffusion coefficients as visible in Figure 12. The discrepancy between D_{kk}^{trans} and ${}^{(2)}D_{kk}^{\text{trans}}$ increases from a few percent at low ionic strength up to 40% at the highest ionic strength. It can be explained by the partial suppression of the negative subregion in the correlation functions of the coordinates caused by the decay of the metric from the initial value of unity.

Including the relaxation of the metric separately, i.e., the first approximation in Table 2, results in a smaller overestimation of typically 10% of the diffusion coefficients for the ions. For water, however, the deviations become larger, in particular for ${}^{(1)}D_{33}^{\text{trans}}$, because of the faster relaxation of the metric as visible in Figure 10. In the case of the off-diagonal elements, this product approximation fails because the metric stays close to zero for too long a time. As the above analysis has revealed the importance of the off-diagonal terms at higher ionic strength, inclusion of the metric is essential.

2. Decomposition of Rotational Motion. Traditionally, the angular velocity $\omega(t)$ is given in terms of Eulerian angles, quaternions, etc. As our definition of the rotation of a pseudorigid body is based on the least-squares fit algorithm of Horn,³⁸ we infer $\omega(t)$ directly from the off-diagonal elements of $W(t)$ in eq 9. The respective rotational diffusion coefficients of the solvent molecules are depicted in Figure 13. In addition to the typical oscillatory character of the underlying correlation functions, high frequency undulations can be detected. Their origin can be traced back to the construction of the rotation matrix by the Horn algorithm. The power spectra of the

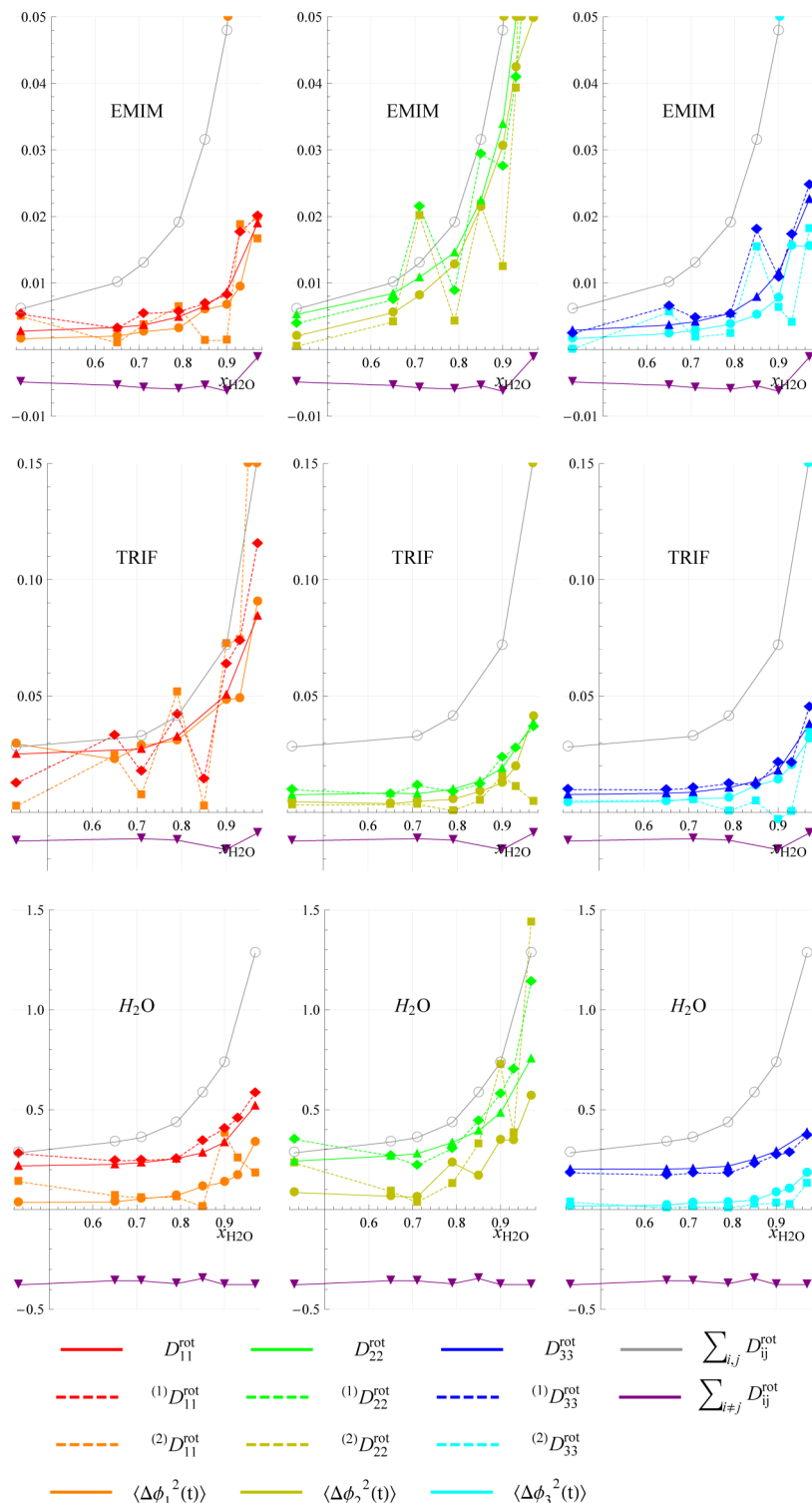


Figure 15. Partial rotational diffusion coefficients (diffusion tensor elements), D_{kk}^{rot} , and approximations, $(^1)D_{kk}^{\text{rot}}$ and $(^2)D_{kk}^{\text{rot}}$, as well as the sum of the off-diagonal elements and the total sum, the rotational diffusion coefficient (times three). Diffusion coefficients from $\langle \Delta\phi_k^2(t) \rangle$ share the color code of the respective $(^2)D_{kk}^{\text{rot}}$ but are given as solid lines.

rotational correlation functions in Figure 13 are shown in Figure 14: For EMIM, the high frequency peak appears in the region of 160 THz for $k = 2$ and 250 THz for $k = 1$ and 3. For TRIF, the peak is at 120 THz for $k = 1$ and 50 THz for $k = 2$ and 3. The intramolecular geometry of water was kept fixed (TIP3 water model). Consequently, the high frequency peak is absent. In general, the increase of ionic strength may change the

amplitude of the sharp high frequency peak but does not alter its position, while the broad low frequency peak is shifted to higher frequencies. Therefore, we conclude that the high frequency peak represents remnant features of intramolecular vibrations handed over by the least-squares fit of the Horn algorithm. They are averaged out upon integration when computing the diffusion coefficients. The low frequency

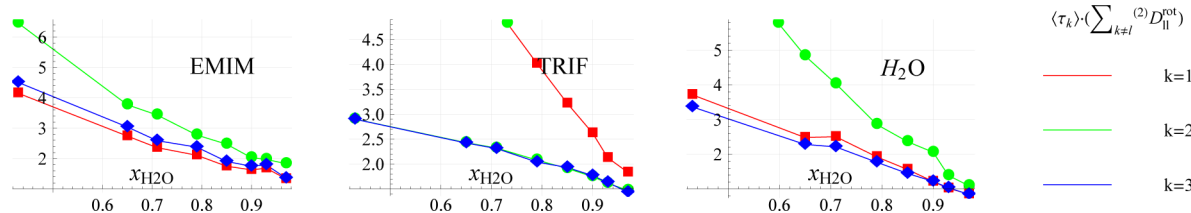


Figure 16. Product of the relaxation time of an axis times the sum of the diffusion coefficients for rotation about the other two axes.

oscillations are definitely of intermolecular character as they shift with the variation of ionic strength.

Figure 15 shows diagonal contributions to the rotational diffusion coefficients for the solvent molecules as a function of the water mole fraction. From the time behavior of the different rotational axes, TRIF seems to be an exact symmetric top with two equivalent axes $k = 2$ and 3 , EMIM is fairly close to a symmetric top with two similar axes $k = 1$ and 3 , and water behaves as a general top with three different axes. Figure 15 also compares the various approximations of Table 2 in the case of rotation. Here, the same trend as for the translational diffusion coefficients is observed: $(^2)D_{kk}^{\text{rot}} < (^1)D_{kk}^{\text{rot}} \approx D_{kk}^{\text{rot}}$. However, the diffusion coefficients $(^2)D_{kk}^{\text{rot}}$ can also be obtained by eq 22, i.e., from the linear slope of the angular displacement $\langle \Delta\phi_k^2(t) \rangle$ (see Supporting Information for the angular displacement curves). These values in Figure 15 almost coincide with $(^2)D_{kk}^{\text{rot}}$ gained from the angular velocity correlation functions at various water mole fractions, but their statistical quality seems to be superior compared to the values obtained from the angular velocity correlation functions. This is somewhat puzzling because the third column in Figure 13 shows nicely converging diffusion coefficients. One has to bear in mind, however, that these results have been obtained including the metric whose relaxation damps the integrand in the asymptotic time regime. Once this metric is neglected, as in $(^2)D_{kk}^{\text{rot}}$, the integral becomes noisy and loses statistical quality.

The cumulant expansion in eq 19 postulates that the product of the relaxation time of an axis times the sum of the diffusion coefficients for rotation about the other two axes should be unity. Figure 16 checks this postulate: It is found to be valid for high water mole fractions but breaks down at higher ionic strength. Apart from the question of validity of the cumulant expansion for ionic liquids whose complexity implies multi-exponential behavior, there are two possible explanations: On the one hand, the relaxation times $\langle \tau_k \rangle$ for the axis coinciding with the dipole moment vector obey viscosity scaling. The complementary diffusion coefficients, however, do not. Therefore, the product cannot remain constant, i.e., be independent of the ionic strength. On the other hand, the increasing importance of the off-diagonal elements of the diffusion tensor cannot be ignored.

V. CONCLUSION

Hydrated ionic liquids can be still characterized by a charge ordering function, but the dielectric screening effect of the water dipoles results in a shorter range of this cation–anion network. The intruding water molecules seem to form a network with the anions: They prefer positions near the hydrophilic sulfonyl group of the trifluoromethanesulfonate anions. The next trifluoromethanesulfonate anions point with their sulfonyl group toward these water molecules forming a bridged structure TRIF–water–TRIF. As a result, the anionic dipoles are aligned in an antiparallel fashion, and the interstitial

water acts as a glue for this typical configuration. In contrast to the kosmotropic anions, the imidazolium cations are expelled from this water–anion network. Consequently, they aggregate in hydrophobic clusters or accumulate in the direct solvation shell of biomolecular solutes, if present. The accumulation can be determined by an increased coordination number of cations at the surface of proteins, even if the protein is positively charged. The hydrophobic clusters can be detected for example by the decreasing contact distance between cations, i.e., the radial distribution function $g_{\text{EMIM-EMIM}}^{000}(r)$, with increasing water mole fraction. As a result, a simple characterization of an ionic liquid in terms of kosmotropic or chaotropic behavior is not possible when describing its effect on the protein stability: The anions act kosmotropically, whereas the imidazolium cations show chaotropic behavior. It seems that the structural changes of the hydration shell are of minor importance for the stability of a protein; e.g., the mutual orientation of water dipoles is only slightly influenced by the presence of a protein since the distance-dependent Kirkwood factors $G_k(R)$ look alike. In fact, the enrichment of cations on the protein surface and the tight binding of anions to specific spots on the protein surface play a more crucial role for the protein stability.

Nevertheless, the structure of water molecules in the solvation shell lasts for long distances in the presence of ionic liquids. For example, at a water mole fraction of $x_{\text{H}_2\text{O}} = 0.68$, the mutual orientation of water molecules can be detected for more than 20 Å as shown by the respective Kirkwood factor $G_k(R)$. The different characters of the three solvent species are also reflected in the long-distance limit of the Kirkwood factor G_k : close to unity, below unity, and above unity for imidazolium cations, trifluoromethanesulfonate, and water, respectively. This factor determines the correlation between molecular dipole rotation and collective rotation, i.e., the Kievelson–Madden relation, in the ionic liquid/water mixtures without a biomolecular solute. The collective rotation of water is slower compared to the molecular reorientation of water dipoles. In contrast, the collective rotation of the anions is faster than the corresponding molecular reorientation. However, this relation is spoiled by solvent molecules bound to the solute in the SZNF and 1UBQ systems. Computation of a modified G_k factor, freed from the impact of bound molecules, enables a modified Kievelson–Madden relation.

The translational (motion of the center of mass) and rotational (reorientation of the dipolar axis) single particle dynamics seems to follow hydrodynamic rules; i.e., respective motional parameters obey viscosity scaling. In contrast, this viscosity scaling does not apply for axes perpendicular to the dipolar axes. Introducing a body-fixed frame as an alternative to the usual laboratory frame, single particle translation and reorientation can be analyzed in higher detail: The translational and rotational diffusion coefficients can be decomposed into contributions along, or from, different molecular axes. To the

best of our knowledge, this is the first ionic liquid study of such a systematic decomposition in the body-fixed frame. Correlations between different axes, the so-called off-diagonal terms, increase with increasing ionic strength. They reduce the overall diffusion coefficient because of their negative sign. Thus, the small translational and rotational diffusion coefficients of pure ionic liquids are caused by the strongly correlated motion along different axes. The so-called cumulant expansion links the rotation about axes with the rotation of axes. However, it only works at very high water mole fractions. All in all, the relaxation of the metric, i.e., the reorientation of the body-fixed frame, is essential for rotational as well as translational diffusion coefficients.

■ ASSOCIATED CONTENT

Supporting Information

We describe the translational and rotational dynamics of the solutes with respect to the body-fixed frame. Furthermore, the mean-squared angular displacement of the solvent species is given at all water mole fractions. This information is available free of charge via the Internet at <http://pubs.acs.org>.

■ AUTHOR INFORMATION

Corresponding Author

*E-mail: os@mdy.univie.ac.at.

Notes

The authors declare no competing financial interest.

■ ACKNOWLEDGMENTS

The computational work was performed on the “Vienna Scientific Cluster” (www.zid.tuwien.ac.at/vsc) of the University of Vienna, the Vienna University of Technology, and the University of Natural Resources and Applied Life Science Vienna. We thank them for the generous allocation of computer time. This work was supported by Project No. P19807 of the FWF Austrian Science Fund.

■ DEDICATION

This paper is dedicated to Prof. Wilfred van Gunsteren on occasion of his 65th birthday, honoring his outstanding and stimulating scientific oeuvre.

■ REFERENCES

- (1) Hermanutz, F.; Meister, F.; Uerdingen, E. *Chem. Fibers Int.* **2006**, *6*, 342.
- (2) Ressmann, A. K.; Gaertner, P.; Bica, K. *Green Chem.* **2011**, *13*, 1442.
- (3) Ressmann, A. K.; Strassl, K.; Gaertner, P.; Zhao, B.; Greiner, L.; Bica, K. *Green Chem.* **2012**, *14*, 940.
- (4) Stoimenovski, J.; Dean, P. M.; Izgorodina, E. I.; MacFarlane, D. R. *Faraday Discuss.* **2012**, *154*, 335.
- (5) Halle, B. *Philos. Trans. R. Soc. London, Sect. B* **2004**, *359*, 1207.
- (6) Schröder, C.; Rudas, T.; Boresch, S.; Steinhauser, O. *J. Chem. Phys.* **2006**, *124*, 234907.
- (7) Zhang, Y.; Furyk, S.; Bergreiter, D. E.; Cremer, P. S. *J. Am. Chem. Soc.* **2005**, *127*, 14505.
- (8) Russo, D. *Chem. Phys.* **2008**, *345*, 200.
- (9) Yang, Z. *J. Biotechnol.* **2009**, *144*, 12.
- (10) Zhang, Y.; Cremer, P. S. *Annu. Rev. Phys. Chem.* **2010**, *61*, 63.
- (11) Gurau, M. C.; Lim, S.-M.; Castellana, E. T.; Albertorio, F.; Kataoka, S.; Cremer, P. S. *J. Am. Chem. Soc.* **2004**, *126*, 10522.
- (12) Parsons, D. F.; Boström, M.; Nostro, O. L.; Ninham, B. W. *Phys. Chem. Chem. Phys.* **2011**, *13*, 12352.
- (13) Kowacz, M.; Mukhopadhyay, A.; Cravalho, A. L. M.; Esperanca, J. M. S. S.; Romao, M. J.; Rebelo, L. P. N. *Cryst. Eng. Comm.* **2012**, DOI: 10.1039/C2CE25129A.
- (14) Omta, A. W.; Kropman, M. F.; Woutersen, S.; Bakker, H. J. *Science* **2003**, *301*, 347.
- (15) Freire, M. G.; Carvalho, P. J.; Silva, A. M. S.; Santos, L. M. N. B. F.; Rebelo, L. P. N.; Marrucho, I. M.; Coutinho, J. A. P. *J. Phys. Chem. B* **2009**, *113*, 202.
- (16) Tomé, L. I. N.; Jorge, M.; Gomes, J. R. B.; Coutinho, J. A. P. *J. Phys. Chem. B* **2010**, *114*, 16450.
- (17) Klähn, M.; Lim, G. S.; Seduraman, A.; Wu, P. *Phys. Chem. Chem. Phys.* **2011**, *13*, 1649.
- (18) Haberler, M.; Schröder, C.; Steinhauser, O. *Phys. Chem. Chem. Phys.* **2011**, *13*, 6955.
- (19) Haberler, M.; Steinhauser, O. *Phys. Chem. Chem. Phys.* **2011**, *13*, 17994.
- (20) Micaeló, N. M.; Soares, C. M. *J. Phys. Chem. B* **2008**, *112*, 2566.
- (21) Cammarata, L.; Kazarian, S. G.; Salter, P. A.; Welton, T. *Phys. Chem. Chem. Phys.* **2001**, *3*, 5192.
- (22) Hanke, C. G.; Lynden-Bell, R. M. *J. Phys. Chem. B* **2003**, *107*, 10873.
- (23) Jiang, W.; Wang, Y.; Voth, G. A. *J. Phys. Chem. B* **2007**, *111*, 4812.
- (24) Schröder, C.; Steinhauser, O. *J. Chem. Phys.* **2010**, *132*, 244109.
- (25) Neumayr, G.; Schröder, C.; Steinhauser, O. *J. Chem. Phys.* **2009**, *131*, 174509.
- (26) Liu, H.; Sale, K. L.; Simmons, B. A.; Singh, S. *J. Phys. Chem. B* **2011**, *115*, 10251.
- (27) Tran, C. D.; De Paoli Lacerda, S. H.; Oliveira, D. *Appl. Spectrosc.* **2003**, *57*, 152.
- (28) Schröder, C.; Rudas, T.; Neumayr, G.; Benkner, S.; Steinhauser, O. *J. Chem. Phys.* **2007**, *127*, 234503.
- (29) Schröder, C.; Neumayr, G.; Steinhauser, O. *J. Chem. Phys.* **2009**, *130*, 194503.
- (30) Lopes, J. N. A. C.; Pádua, A. A. H. *J. Phys. Chem. B* **2006**, *110*, 3330.
- (31) Brooks, B. R.; Brooks, C. L.; Mackerell, A. D.; Nilsson, L.; Petrella, R. J.; Roux, B.; Won, Y.; Archontis, G.; Bartels, C.; Boresch, S.; Caflisch, A.; Caves, L.; Cui, Q.; Dinner, A. R.; Feig, M.; Fischer, S.; Gao, J.; Hodoscek, M.; Im, W.; Kuczera, K.; Lazaridis, T.; Ma, J.; Ovchinnikov, V.; Paci, E.; Pastor, R. W.; Post, C. B.; Pu, J. Z.; Schaefer, M.; Tidor, B.; Venable, R. M.; Woodcock, H. L.; Wu, X.; Yang, W.; York, D. M.; Karplus, M. *J. Comput. Chem.* **2009**, *30*, 1545.
- (32) Martínez, L.; Andrade, R.; Birgin, E. G.; Martínez, J. M. *J. Comput. Chem.* **2009**, *30*, 2157.
- (33) Canongia Lopes, J. N.; Deschamps, J.; Pádua, A. A. H. *J. Phys. Chem. B* **2004**, *108*, 2038.
- (34) Canongia Lopes, J. N.; Deschamps, J.; Pádua, A. A. H. *J. Phys. Chem. B* **2004**, *108*, 11250.
- (35) Canongia Lopes, J. N.; Pádua, A. A. H. *J. Phys. Chem. B* **2004**, *108*, 16893.
- (36) Hanke, C. G.; Price, S. L.; Lynden-Bell, R. M. *Mol. Phys.* **2001**, *99*, 801.
- (37) MacKerell, A. D.; Bashford, D.; Bellott, M.; Dunbrack, R. L.; Evanseck, J. D.; Field, M. J.; Fischer, S.; Gao, J.; Guo, H.; Ha, S.; Joseph-McCarthy, D.; Kuchnir, L.; Kuczera, K.; Lau, F. T. K.; Mattos, C.; Michnick, S.; Ngo, T.; Nguyen, D. T.; Prodhom, B.; Reiher, W. E.; Roux, B.; Schlenkrich, M.; Smith, J. C.; Stote, R.; Straub, J.; Watanabe, M.; Wiorkiewicz-Kuczera, J.; Yin, D.; Karplus, M. *J. Phys. Chem. B* **1998**, *102*, 3586.
- (38) Horn, B. K. P. *J. Opt. Soc. Am. A* **1987**, *4*, 629.
- (39) Kubo, R. *J. Phys. Soc. Jpn.* **1962**, *17*, 1100.
- (40) Lynden-Bell, R. M.; Steele, W. A. *J. Phys. Chem.* **1984**, *88*, 6514.
- (41) Roy, D.; Patel, N.; Conte, S.; Maroncelli, M. *J. Phys. Chem. B* **2010**, *114*, 8410.
- (42) Berne, B. J.; Pecora, R. *Dynamic Light Scattering*; Dover Publications: Mineola, NY, 2000.
- (43) Schröder, C.; Rudas, T.; Neumayr, G.; Gansterer, W.; Steinhauser, O. *J. Chem. Phys.* **2007**, *127*, 044505.

- (44) Schröder, C.; Rudas, T.; Steinhauser, O. *J. Chem. Phys.* **2006**, 125, 244506.
(45) Kirkwood, J. G. *J. Chem. Phys.* **1939**, 7, 911.
(46) Neumann, M.; Steinhauser, O. *Chem. Phys. Lett.* **1983**, 102, 508.
(47) Madden, P.; Kivelson, D. *Adv. Chem. Phys.* **1984**, 56, 467.
(48) Alder, B. J.; Alley, W. E. *Phys. Today* **1984**, 37, 56.
(49) Schröder, C. *J. Chem. Phys.* **2011**, 135, 024502.
(50) Schröder, C.; Haberler, M.; Steinhauser, O. *J. Chem. Phys.* **2008**, 128, 134501.